Uncovering Mechanisms of Phytoplankton Response to Climate Change

Gwenn M. Miller Hennon

A dissertation

submitted in partial fulfillment of the

requirements for the degree

Doctor of Philosophy

University of Washington

2015

Reading Committee:

E. Virginia Armbrust, Chair

Paul D. Quay

Robert Morris

Program Authorized to Offer Degree:

School of Oceanography

University of Washington

Abstract

Uncovering Mechanisms of Phytoplankton Response to Climate Change

Gwenn M. Miller Hennon

Chair of the Supervisory Committee:
Professor E. Virginia Armbrust
School of Oceanography

Phytoplankton are responsible for approximately half the primary production on earth, fueling marine food webs and driving the cycling of carbon and inorganic nutrients in the oceans. Climate change is predicted to alter the marine environment by elevating carbon dioxide, increasing temperature, and decreasing the availability of inorganic nutrients in the surface ocean where phytoplankton dominate. To predict phytoplankton productivity and abundance in the future requires an understanding of the mechanisms of phytoplankton response to these environmental changes. Here we investigate how a model phytoplankton, *Thalassiosira pseudonana*, acclimates to increasing carbon dioxide through physiological and gene expression changes, and how picophytoplankton communities in the tropical Atlantic respond to variations in temperature and nutrient availability. By uncovering mechanisms of phytoplankton response to environmental variables we gain new insights into predicting how marine food webs and biogeochemical cycles may be altered by climate change.

Table of Contents

Introduction

The global carbon cycle has been strongly perturbed by human activities including burning fossil fuels and changes in land use, which have increased oxidation of organic carbon deposits at ~100x the natural rate[1]. The resulting emissions of CO_2 to the atmosphere currently total ~9 Pg C yr^{-1} with roughly half of the emissions absorbed by the ocean[2]. Atmospheric CO_2 warms the planet due to its absorption of infrared light[3], and CO_2 that dissolves into the ocean results in wide spread acidification and shifts the balance of marine carbonate chemistry[4,5]. These changes to global temperatures and marine chemistry are predicted to increase throughout this century at a rate unprecedented in the geologic record[6], likely leading to wide scale changes in marine ecosystems.

Approximately half of global primary production is due to marine phytoplankton[7]. Phytoplankton-derived organic matter forms the base of the marine food web and also drives the biological carbon pump when it sinks into the ocean interior[8]. Phytoplankton, unlike terrestrial plants, are rapidly produced and consumed leading to a smaller total biomass and an extremely fast turn over time[9]. Consequently, phytoplankton communities respond rapidly to environmental changes and have a surprising diversity of forms[10], due to high genetic diversity and metabolic flexibility that allows phytoplankton acclimate and adapt to environmental changes. Climate change is expected to impose a myriad of changes on the marine environment including ocean acidification, warming, and increased stratification[11]. These changes are predicted to alter the structure of phytoplankton communities and the biological pump[12] but many questions remain as to the magnitude and direction of these changes.

One source of uncertainty in predicting the response of phytoplankton to environmental change is the extent of flexibility in phytoplankton physiology, which allows for acclimation to change. Acclimation is a shift in phytoplankton physiology due to changes in gene expression. In contrast to adaptation, it does not require genes to mutate or be exchanged. Several studies examined acclimation and adaptation of phytoplankton in response to elevated CO_2[13–15], but responses varied widely and the mechanism of how a phytoplankton cell senses and acclimates to CO_2 remains largely unknown. In Chapters 1 and 2 we explore how a model phytoplankton acclimates to rising CO_2 and which genes and metabolic pathways are responsible for the acclimation response.

Another source of uncertainty is how field populations differ from laboratory strains and how combinations of environmental factors influence phytoplankton growth and abundance in the ocean. Field studies can also provide more information about the range of metabolic capabilities in phytoplankton and the geographic distribution of different ecotypes. Current ecosystem models rely on parameters derived from relatively few phytoplankton strains[16] and therefore may be subject to culturing bias or miss important metabolic diversity[17]. In Chapter 3 we examine natural populations of the smallest and most abundant phytoplankton, cyanobacteria, to investigate the range of physiology across temperature and nutrient gradients in the tropical Atlantic.

Insights gained from studies of model phytoplankton and field populations can be integrated to improve models of phytoplankton, community structure, productivity and the consequences for biogeochemical cycles. By investigating the mechanisms of phytoplankton responses to climate change we can improve these model predictions and

thereby improve our ability to forecast future fisheries and shifts in the marine carbon cycle.

1. Berner, R. A. The long-term carbon cycle, fossil fuels and atmospheric composition. *Nature* **426,** 323–326 (2003).

2. Le Quéré, C. *et al.* The global carbon budget 1959–2011. *Earth Syst. Sci. Data Discuss.* **5,** 1107–1157 (2012).

3. Meehl, G. A. *et al. Global climate projections*. *Climate change* (2007). at <http://www.ipcc.ch/publications_and_data/ar4/wg1/en/ch10.html>

4. Sabine, C. L. *et al.* The oceanic sink for anthropogenic CO_2. *Science* **305,** 367–71 (2004).

5. Feely, R. a *et al.* Impact of anthropogenic CO2 on the CaCO3 system in the oceans. *Science* **305,** 362–6 (2004).

6. Honisch, B. *et al.* The Geological Record of Ocean Acidification. *Science (80-.).* **335,** 1058–1063 (2012).

7. Field, Christopher B., Behrenfeld, Michael J., Randerson, James T., Falkowski, P. Primary Production of the Biosphere: Integrating Terrestrial and Oceanic Components. *Science (80-.).* **281,** 237–240 (1998).

8. Ducklow, H. W., Steinberg, D. K. & Buesseler, K. O. Upper Ocean Carbon Export and the Biological Pump. *Oceanography* **14,** 50–58 (2001).

9. Falkowski, P. G., Barber, R. T. & Smetacek, V. Biogeochemical Controls and Feedbacks on Ocean Primary Production. *Science (80-.).* **281,** 200–206 (1998).

10. Hutchinson, G. E. The Paradox of Plankton. *Am. Nat.* **95,** 137–145 (1961).

11. Hoegh-Guldberg, O. *et al. The Ocean. In: Climate Change 2014: Impacts, Adaptation, and Vulnerability. Part B: Regional Aspects. Contribution of Working Group II to the Fifth Assessment Report of the Intergovernmental Panel on Climate Change*. (2014).

12. Riebesell, U., Körtzinger, A. & Oschlies, A. Sensitivities of marine carbon fluxes to ocean change. *Proc. Natl. Acad. Sci. U. S. A.* **106,** 20602–9 (2009).

13. Collins, S. & Bell, G. Phenotypic consequences of 1,000 generations of selection at elevated CO2 in a green alga. *Nature* **431,** 566–9 (2004).

14. Lohbeck, K. T., Riebesell, U. & Reusch, T. B. H. Adaptive evolution of a key phytoplankton species to ocean acidification. *Nat. Geosci.* **5,** 346–351 (2012).

15. Tatters, A. O. *et al.* Short- and long-term conditioning of a temperate marine diatom community to acidification and warming. *Philos. Trans. R. Soc. Lond. B. Biol. Sci.* **368,** 1–14 (2013).

16. Follows, M. J., Dutkiewicz, S., Grant, S. & Chisholm, S. W. Emergent biogeography of microbial communities in a model ocean. *Science* **315,** 1843–1846 (2007).

17. Martiny, A. C., Kathuria, S. & Berube, P. M. Widespread metabolic potential for nitrite and nitrate assimilation among Prochlorococcus ecotypes. *Proc. Natl. Acad. Sci. U. S. A.* **106,** 10787–92 (2009).

Chapter 1:

ACCLIMATION CONDITIONS MODIFY PHYSIOLOGICAL RESPONSE OF THE DIATOM *THALASSIOSIRA PSEUDONANA* TO ELEVATED CO_2 CONCENTRATIONS IN A NITRATE-LIMITED CHEMOSTAT

Authors: Gwenn M. M. Hennon, Paul Quay, Rhonda L. Morales, Lyndsey M. Swanson, E. Virginia Armbrust

Reproduced with permission from:

Journal of Phycology

John Wiley and Sons

Abstract

Diatoms are responsible for a large proportion of global carbon fixation, with the possibility that they may fix more carbon under future levels of high CO_2. To determine how increased CO_2 concentrations impact the physiology of the diatom *Thalassiosira pseudonana* (Hustedt) Hasle et Heimdal, nitrate-limited chemostats were used to acclimate cells to a recent past (333 ± 6 μatm) and two projected future concentrations (476 ± 18 μatm, 816 ± 35 μatm) of CO_2. Samples were harvested under steady-state growth conditions after either an abrupt (15-16 generations) or a longer acclimation process (33-57 generations) to increased CO_2 concentrations. The use of un-bubbled chemostat cultures allowed us to calculate the uptake ratio of dissolved inorganic carbon relative to dissolved inorganic nitrogen (DIC:DIN), which was strongly correlated with fCO_2 in the shorter acclimations but not in the longer acclimations. Both CO_2 treatment and acclimation time significantly affected the DIC:DIN uptake ratio. Chlorophyll *a* per cell decreased under elevated CO_2 and the rates of photosynthesis and respiration decreased significantly under higher levels of CO_2. These results suggest that *T. pseudonana* shifts carbon and energy fluxes in response to high CO_2 and that acclimation time has a strong effect on the physiological response.

Introduction

Burning fossil fuels and changes in land use have accelerated the oxidation of organic carbon deposits by about two orders of magnitude above natural levels (Berner, 2003), currently corresponding to the release of ~9 Pg of carbon per year into the atmosphere (Le Quéré et al. 2012). The concentration of CO_2 in the atmosphere has increased from a pre-industrial 280 μatm, to the present 400 μatm, and is predicted to rise to 500-1000 μatm by the year 2100 (Meehl, et al. 2007). The ocean acts as a sink for anthropogenic carbon, taking up about 1.6 Pg C yr^{-1} (Takahashi et al. 2009). This process increases the pCO_2 and decreases the buffering capacity and pH of the ocean resulting in ocean acidification (Sabine et al. 2004; Denman et al. 2007). In the geologic record, large extinction events of ocean life have been associated with previous events of carbon dioxide flux into the oceans (Hönisch et al. 2012) so the recent more rapid rate of CO_2 emission may have profound effects on ocean ecosystems.

Diatoms fix ~20 Pg of carbon every year, accounting for ~20% of global primary productivity (Sarmiento and Gruber 2002; Nelson et al. 1995). Some of this carbon escapes degradation and is buried in seafloor sediments leading to long-term carbon sequestration (Berner, 2003). If diatoms and other phytoplankton fix more carbon per limiting nutrient in response to increased ocean pCO_2 (Riebesell et al. 2009), this could potentially result in a negative feedback on the atmospheric CO_2 increase as a fraction of this additional fixed carbon would be sequestered in the deep ocean (Denman et al.2007). It remains an open question as to whether phytoplankton will increase carbon fixation rates under elevated CO_2 because nutrient supply often limits production (Moore et al.

2002) and phytoplankton may acclimate to higher CO_2 concentrations by decreasing the production of reducing equivalents rather than increasing carbon fixation.

Diatoms and nearly all other marine algae use carbon-concentrating mechanisms (CCMs) to concentrate CO_2 at the site of carbon fixation because of the poor affinity of the enzyme RUBISCO for CO_2 (Badger et al. 1998; Reinfelder, 2011; Raven et. al 2012). CCMs are energetically expensive, requiring an estimated additional 1.5-6 ATP per carbon fixed equating to a 13-51% increase in the cost of C fixation in addition to the energy required for protein production and maintenance (Hopkinson et al. 2011). CCMs are also important for reducing the oxygenase activity of RUBISCO, which results in the fixation of oxygen or photorespiration and consumes 1-2 ATP, 1 fixed carbon, and 1-2 NADH (Raven et. al 2012; Bauwe et al. 2010). Under elevated CO_2, diffusion of CO_2 supplies a greater pool of inorganic carbon to RUBISCO, resulting in a decrease in photorespiration rates and reliance on CCMs (Badger et al. 1998; Burkhardt et al. 2001, Trimborn et al. 2009). A decrease in CCM activity and photorespiration rates under future CO_2 would alter the fluxes of energy equivalents (e.g., NADH and ATP) and potentially also carbon within the cell (Raven and Johnston 1991). Changes in CO_2 concentration may also shift the competitive advantage between phytoplankton groups (Raven and Johnston 1991) resulting in changes in population cell size and/or biomineralization, altering the sinking rate of organic carbon to depth (Finkel et al. 2009).

Multiple physiological responses of phytoplankton have been elicited under experimentally increased pCO_2, but with little consensus on magnitude or direction. Under high pCO_2, plankton communities in some experimental mesocosms increased carbon uptake by ~40% (Riebesell et al. 2007), while in other mesocosms, the plankton

communities did not increase uptake and instead shifted from particulate organic carbon (POC) to dissolved organic carbon (DOC) production (Kim et al. 2011). In yet other mesocosms, the community composition shifted towards plankton with larger average cell sizes with no significant change in carbon fixation (Engel et al. 2008).

To assess the contribution of diatoms to the changes in carbon fluxes, we chose to use a well-studied cultured representative, *Thalssiosira pseudonana* (Hasle and Heimdal 1970). Previous studies with the diatom *T. pseudonana* under elevated CO_2 have documented changes in the cellular carbon and electron transport, but have shown variable results depending on culture conditions. For example, *T. pseudonana* exhibited no change in CO_2 half-saturation concentration after 5-6 generations of acclimation to high CO_2 in batch culture (Trimborn et al. 2009). Sobrino et al. (2008) found that cells possessed decreased amounts of chlorophyll *a* in semi-continuous cultures after about 12 generations under high CO_2 while McCarthy et al. (2012) found no change in chlorophyll *a* content per cell after 7.5 generations of growth under high CO_2. Both studies found that *T. pseudonana* appeared to change electron transport rates with Sobrino et al (2008) finding a higher susceptibility to oxidative stress in short-term batch cultures with high CO_2 and McCarthy et al. (2012) finding that the rate of photosystem II repair increased. Dramatically different results were obtained when *T. pseudonana* cells were maintained under high CO_2 for longer periods of time. After 20 generations of exponential growth at high CO_2, the half-saturation concentration for CO_2 increased, presumably due to decreased CCM (Yang and Gao, 2012). After 100 generations of continuous culture at high CO_2, the number of transcripts associated with CCM components decreased and chlorophyll *a* per cell increased (Crawfurd et al. 2011).

Experiments on other cultured groups of algae have also found variable responses depending on acclimation time. The green alga, *Chlamydomonas reinhardtii*, decreased cell size and increased photosynthesis and respiration rates after 1000 generations of growth in high CO_2 batch cultures (Collins and Bell 2004). Conditioning time, rather than CO_2 level, was shown to have the strongest effect on the outcome of competition experiments between dinoflagellate isolates over 35-120 generations (Tatters et al. 2012), although the same result was not found with diatom assemblages (Tatters et al. 2013). In a long-term batch culture study with *E. huxleyi*, cell growth rates and calcification were depressed under elevated CO_2, but the effect was diminished after 500 generations of selection (Lohbeck et al. 2012). These types of long duration experiments are rare, but they provide a valuable look at how selection and adaptation could change the physiology of future algal populations.

Nutrient limitation has also been shown to modulate the effects of CO_2 on algal physiology. Diatoms of the genus *Attheya* grew faster and fixed more carbon under high CO_2 and nutrient-replete conditions, yet vitamin B_{12} limitation caused all cultures to grow at the same rate regardless of CO_2 treatment (King et al. 2011). The diatom *Phaeodactylum tricornutum* significantly increased the ratio of cellular C:N under high CO_2 and nitrate limitation compared to nutrient replete cultures (Li et al. 2012). The coccolithophorid, *Emiliania huxleyi* decreased cell volume under high CO_2 in a phosphate-limited chemostat (Borchard et al. 2011), yet in a nutrient replete batch culture experiment by Iglesias-Rodriguez et al. (2008) the cells increased in volume and were more heavily calcified with an increased Redfield ratio. Another study with *E. huxleyi*

found different trends in cellular calcification under elevated CO_2 with nitrate and phosphate starvation compared to nutrient replete cultures (Ruoco et al. 2013).

The physiological responses of marine algae vary with culturing method, nutrient limitation and acclimation time. We hypothesized that under high CO_2 *Thalassiosira pseudonana* would down-regulate CCMs, resulting in an increase in available energy equivalents and a compensatory down-regulation of energy producing processes. We also hypothesized that longer acclimations, with slower changes in fCO_2, would reduce cell oxidative stress and result in a moderated physiological response. We chose nitrate-limited chemostats to test the acclimated physiology of the diatom *T. pseudonana* to high CO_2 because this method provides a good approximation of ocean-relevant conditions; in most of the ocean regions where diatoms dominate, nitrate availability limits growth (Moore et al. 2002). Nitrate-limited chemostats also allow for greater control of culture conditions by maintaining culture biomass, nutrients and gases such as CO_2 at relatively stable levels for many generations (LaRoche et al. 2010).

Materials and Methods

Culture conditions. Axenic *Thalassiosira pseudonana* (strain CCMP 1335) was obtained from the National Center for Marine Algae and Microbiota. Chemostats were run in duplicate polycarbonate bottles under continuous light (83 ± 3 μmol photons m^{-2} s^{-1}) and 20°C for two different durations for a total of four biological replicates per CO_2 concentration. In the "short" chemostat runs, cells came to acclimation at the target CO_2 concentration after 15-18 generations. In the "long" chemostat runs, cells were first acclimated to low (330 μatm) CO_2 for 9-18 generations and then ramped up to the target

CO_2 levels over the course of 5-6 generations then re-acclimated for a total of 33-57 generations in culture. The chemostats were mixed continuously with a stir bar, and the volume was maintained at 1.00L ± .05 using a water-trap drain outflow to maintain sterility and minimize gas exchange (Figure 1). The growth rate was limited by the dilution rate to 1.61 ± .22 day^{-1} (~70% of maximum growth rate at the same irradiance) using a Peri-Star Pro peristaltic pump (World Precision Instruments Inc. Sarasota, FL). The culture biomass was limited to 1.5 ± 0.4 $x10^5$ cells/mL by the media supply of 10 μM NO_3 which was depleted to < 0.6 μM NO_3 in each chemostat. The media was autoclaved artificial seawater, ESAW recipe (Berges et al. 2001), with f/2 nutrients (except low 10 μM NO_3), corrected with sodium bicarbonate to a final alkalinity of 2200-2300 μmoles/kg as determined by pH and DIC measurements (see *Carbonate chemistry measurements*). Laboratory air was stripped of water with Du-cal (Drierite company, Xenia, OH) and CO_2 with Sodasorb (Divers Supply Inc., Gretna, LA) and mixed with 99.99% pure CO_2 (Praxair, Danbury, CT) using mass flow controllers (GFC-17, Aalborg, Orangeburg, NY) and checked with a CO_2 analyzer (Qubit).

Sampling and analyses. Daily samples (chlorophyll *a* fluorescence, F_v/F_m, cell concentrations, pH and DIC) comprised less than 10% of the culture volume and were collected through a syringe port to prevent bacterial contamination of the chemostats and media. After at least 10 generations of growth under the same CO_2 concentration, the cultures were monitored for a minimum of three consecutive days (5 generations) until less than a 10% change was observed for chlorophyll *a* fluorescence, photosynthetic efficiency (F_v/F_m) and fCO_2. When these conditions were met the chemostats were assumed to be at steady state and were harvested.

Fluorescence, F_v/F_m and cell concentrations. We determined chlorophyll *a* fluorescence with a 10-AU fluorometer (Turner Designs, Sunnyvale, CA), photochemical yield of photosystem II (F_v/F_m) in triplicate with a Phyto-PAM fluorometer (WALZ, Effeltrich, Germany), and cell concentrations by counting three subsamples with a hemocytometer (Fisher Sci). On the day of harvest, we determined cell concentration with the flow cytometer for better statistical power (see *flow cytometry measurements*).

Carbonate chemistry measurements. Dissolved inorganic carbon (DIC) was measured with an AS-C3 DIC analyzer (Apollo SciTech Inc., Bogart, GA) calibrated daily with certified reference materials (Andrew Dickson, UCSD). pH was measured using m-cresol purple dye (Acros Organics) according to the protocol of Dickson et al (2007) and accuracy was checked with pH standards (Andrew Dickson, UCSD). The fCO_2, alkalinity and Revelle factor were calculated using CO2SYS software (Lewis and Wallace http://cdiac.ornl.gov/oceans/co2rprt.html).

The DIC drawdown (DIC deficit of the chemostats compared to the media) was corrected for CO_2 gas leakage through the silicon tubing. The leak rate was determined by the difference between the DIC measured in the media and in sterile chemostat bottles after at least one day of stable flow and prior to the addition of cells. We measured a leak of CO_2 from the tubing connecting the media bottle to the chemostat vessel (Figure 1) as 15.8 ± 3.7 μmoles kg^{-1} day^{-1} (0.4%), 42.7 ± 2.7 μmoles kg^{-1} day^{-1} (1.2%), and 144.3 ± 1.0 μmoles kg^{-1} day^{-1} (4.1%) for low, medium and high CO_2 conditions respectively. The leak rate under the high CO_2 condition was confirmed to be the same before and after the two months of high CO_2 experiments, giving us confidence that the leak rates did not worsen over time. The biological DIC drawdown was calculated by averaging the last

three days of DIC deficit, subtracting the DIC leak, and subtracting the slope fit to the last four days of DIC concentrations in the chemostat to correct for any trend in DIC supply caused by fluctuations of total alkalinity in the media.

Particulate organic carbon (POC), particulate nitrogen (PN), nutrient measurements. POC and PN samples were filtered directly from the chemostat and media bottles onto pre-combusted GFF filters and frozen at -20°C until analysis. Nutrient samples were collected directly from the chemostat and media bottles and filtered through a sterile 0.2 μm syringe filter and frozen at -20°C until analysis. The samples were analyzed using a CE-440 CHN analyzer (Exeter Analytical) for POC/PN measurements and a Technicon AAII system for nutrients according to the protocols of the WOCE Hydrographic Program. Measurements of POC/PN and inorganic nitrogen (the sum of nitrate, nitrite and ammonia) in the media were subtracted from chemostat measurements to get POC/PN production rates and dissolved inorganic nitrogen (DIN) uptake rates.

Photosynthesis and respiration rate measurements. Photosynthesis and respiration rates were estimated using measurements of the isotopic composition of dissolved O_2 and the O_2/Ar dissolved gas ratio (Quay et al., 1993). Pre-evacuated vacuum flasks were used to collect gas samples and the isotope composition ($^{18}O/^{16}O$) and oxygen to argon ratio (O_2/Ar) of the dissolved oxygen gas was determined by mass spectrometer (MAT253) following the procedure of Barkan and Luz (2003). The O_2/Ar ratio was used to calculate the concentration of dissolved oxygen assuming that the argon gas was in equilibrium with air for the measured salinity and temperature of the media. The $^{18}O/^{16}O$ of photosynthetically produced O_2 depends on the $^{18}O/^{16}O$ of the water in the media, which was measured by mass spectrometry (Micromass Isoprime). The oxygen photosynthesis

and respiration rates were determined using steady state O_2 mass and isotope budgets for the chemostat described by the following equations:

(1) $$\frac{d[O_2]}{dt} = [O_2]_{in} * F + P - [O_2]_{out} * F - R = 0$$

$$\frac{d[O_2]}{dt} = [O_2]_{in} * F + P - [O_2]_{out} * F - R = 0$$

(2) $$\frac{d(^{18}O_2)}{dt} = F * \left[\left(\frac{^{18}O}{^{16}O}\right)_{in} * [O_2]_{in} - \left(\frac{^{18}O}{^{16}O}\right)_{out} * [O_2]_{out}\right] + P * \alpha_P * \left(\frac{^{18}O}{^{16}O}\right)_{water} - R * \left(\frac{^{18}O}{^{16}O}\right)_{out} * \alpha_R = 0$$

$$\frac{d\left(\frac{^{18}O}{^{16}O}\right)}{dt} = F * \left[\left(\frac{^{18}O}{^{16}O}\right)_{in} * [O_2]_{in} - \left(\frac{^{18}O}{^{16}O}\right)_{out} * [O_2]_{out}\right] + P * \alpha_P * \left(\frac{^{18}O}{^{16}O}\right)_{water} - R * \left(\frac{^{18}O}{^{16}O}\right)_{out} *$$

Where P is photosynthesis rate and R is respiration rate (μmoles O_2/min), F is the chemostat flow rate (L/min), $[O_2]$ is the O_2 concentration (umols/L), $^{18}O/^{16}O$ for dissolved O_2 in the media input (in) and output (out) and water (water), $\alpha_R = 0.9806$ (Helman et al. 2005) and $\alpha_P = 1.0045$ (Eisenstadt et al. 2010) and represent the oxygen isotopic fractionation effects during respiration and photosynthesis, respectively. These equations were solved numerically for P and R to yield photosynthesis and respiration rates (fmol O_2 / min) using the solve function (base package the R-project).

To test the sensitivity of our calculations of photosynthesis and respiration rates to alternative oxygen reactions we used previous literature to estimate that photorespiration and the Mehler reaction could consume a maximum of 5% and 20% of photosynthetic oxygen production respectively (Claquin et al. 2004, Laws et al. 2000). The fractionations of $^{18}O/^{16}O$ due to photorespiration and the Mehler reaction are 0.9785 and 0.9900 respectively (Helman et al. 2005). We tested minimum, maximum and declining

rates of photosynthesis and the Mehler reaction with elevated CO_2. We also tested the sensitivity of the calculations to the fractionation of photosynthesis.

Flow cytometry measurements (FCM). All flow cytometry measurements were made with an inFlux flow cytometer (Cytopeia) equipped with a 488 nm laser; measured parameters were forward light scatter (FSC), emission at 692 nm (40 nm band pass) for chlorophyll *a* fluorescence, and side scatter (SSC). Unstained cells were measured within 1hr of their removal from the chemostat. DNA content per cell was determined by staining the same samples with SYBR Green (final dilution $1x10^{-4}$) for 30 minutes and measuring emission at 530 nm (40 nm band pass). The absence of bacterial contamination was confirmed with the SYBR-stained samples. Cell concentrations were obtained by measuring the flow through the inFlux while counting particles; the flow meter was calibrated at the start and end of each set of samples. At least 20,000 cells were counted from each sample. The data from FCM measurements were gated into populations with FlowJo software. All measurements were first normalized to 2μm beads (PolySciences Inc. Warrington, PA) as an internal standard and then to the median of the control cultures used to inoculate the chemostat. Control cultures were grown in semi-continuous batch culture maintained in exponential growth in nutrient replete media at the same light level.

Statistical Analysis. Statistical significance was assessed with one-way or two-way ANOVA (aov function, stats package in R) to account for the effects of CO_2 treatment and acclimation conditions where sufficient replicates were available. To test for statistically significant linear correlations between cell physiology measurements and fCO_2, we used the linear model function to perform an F test (lm, stats R).

Error Analysis. The measurement uncertainty of flow rate and DIC were determined by standard error of at least three technical replicates to be <5% and 0.1% respectively. The measurement uncertainty of POC, PN and nutrients was <1% as determined by standards. Measurement uncertainty was propagated for all calculations and was reported where it exceeded the standard error of biological replicates. The accuracy of DIC and pH measurements was 2 µmol/kg and 0.005 pH units respectively so the uncertainty of the parameters calculated by CO2SYS was 9 µatm in fCO_2, 2.3 µmol/kg in total alkalinity, and 0.07 in the Revelle factor. The standard deviation of the uncertainty of photosynthesis and respiration rates ranged from 6-60 fmol $cell^{-1}$ day^{-1} as determined by Monte Carlo analysis with 1000 simulations drawn from normal distributions approximating the errors in flow rate, $(^{18}O/^{16}O)_{out}$ and $(^{18}O/^{16}O)_{in}$ measurements.

Differential growth rate model. To model the potential for a chemostat cell culture to shift the average phenotype of DIC:DIN given a longer acclimation time, the following equations were used to describe the chemostat system.

(3) $$\frac{dC}{dt} = \mu * C - \frac{f}{V} * C \quad \frac{dC}{dt} = \mu * C - \frac{f}{V} * C$$

(4) $$C = e^{kt}$$

(5) $$\mu = k + \frac{f}{V} \mu = k + \frac{f}{V}$$

The cell concentration in the chemostat is described by equation 3, where the change in cells with respect to time (dC/dt) in the chemostat is equal to the growth rate of those cells, µ (day^{-1}), multiplied by the cell number, C, minus the cells lost to outflow, where f is the flow rate in liters per day and V is the volume in liters. Equation 5 was derived from solving for µ in equation 3 by assuming an exponential function for C (equation 4)

where k is the rate constant (day^{-1}). We assumed that cell phenotypes (DIC:DIN uptake) were passed from mother to daughter cells and that cells with different phenotypes could have different growth rates. The distributions of the cell phenotypes (DIC:DIN uptake) were assumed to be Gaussian with a mean calculated from DIC:DIN uptake data from high CO_2 cultures in short and long acclimations and the standard deviation calculated from biological replicates of the low CO_2 treatment. We used equations 4 and 5 to calculate the differential growth rates required to shift the population DIC:DIN uptake of "short" acclimated cultures to match that of "long" acclimated cultures. The Gaussian DIC:DIN uptake distributions were divided into 150 bins and the growth rate, μ, was calculated for each bin using t = 10 days, which is equal to the additional time under high CO_2 in the "long" compared to the "short" acclimation.

Results

Media was bubbled continuously with air amended to 635 ± 15 μatm (low), 1150 ± 25 μatm (medium) or 2800 ± 100 μatm (high) fCO_2. Cells added to the chemostat vessels drew down the initially high fCO_2 utilizing the inorganic carbon to create biomass over the course of the 1-2 days prior to time zero. After the cells grew to a sufficient biomass, the chemostat flow was turned on, corresponding to time zero (Figure 2). The chemostats came to equilibrium at 330 ± 6 μatm (low), 475 ± 18 μatm (medium), or 816 ± 35 μatm (high) fCO_2 (Table 1). The initial DIC draw down of all cultures as well as the increase in culture biomass was similar between treatments. Thus the differences in the magnitude of initial CO_2 drawdown (Figure 2) reflect differences in the Revelle factor or

buffering properties of the carbonate system, which result in a larger change in fCO_2 for the same change in DIC at higher initial fCO_2 (Sabine et al. 2004).

Over the course of the experiment fCO_2 levels reached steady state in the chemostat cultures (Figure 2). In "short" acclimated cultures the carbonate chemistry of the chemostats came to steady state at the target fCO_2 level (Table 1) in 10-12 days, which equates to 15-18 generations of cell divisions. In "long" acclimated cultures, the cells were first acclimated to low fCO_2 (330 μatm) for 6-12 days (9-18 generations) then the fCO_2 was increased in the media over 3-4 days (5-6 generations) to the target level in the chemostats and the cells were allowed to acclimate for an additional 13-22 days (20-33 generations). No ramp up was required for the low fCO_2 "long" acclimation treatment (Figure 2A) because the target level was equal to the initial acclimation fCO_2; the culture was acclimated for an additional 15 days at low fCO_2.

Acclimated cells were harvested from the chemostats once the chlorophyll *a* fluorescence, photosynthetic efficiency (F_v/F_m) and fCO_2 remained relatively constant for three days (see Methods). We calculated the biological uptake of dissolved inorganic carbon by correcting the DIC drawdown for CO_2 leaks and fluctuations of total alkanlinity (TA) in the media, as described above (Table 2). The biological drawdown of DIC, DIN and the production of particulate organic carbon (POC) and particulate nitrogen (PN) were not significantly affected by fCO_2 or acclimation condition, but displayed a decreasing trend with increasing CO_2 (Figure 3).

Trends in the ratio of DIC to DIN drawdown differed between short and long acclimated cultures (Figure 4). The DIC:DIN drawdown was significantly correlated with fCO_2 in short acclimated cultures ($F_{1,4} = 38.7$, $p < 0.01$), but not in the long acclimated

cultures ($F_{1,4} = 0.54$, $p > 0.1$). We found that fCO_2 treatment, acclimation condition and the interaction of the two terms all had significant effects on the DIC:DIN drawdown ($p < 0.01$, $p < 0.01$, $p < 0.01$ respectively).

Flow cytometry was used to investigate whether there were corresponding differences in cell morphology with the changes in DIC:DIN drawdown. Optical measurements of all cells were normalized to the culture used to inoculate the chemostats (Figure 5). As expected under nitrogen limitation, the acclimated chemostat cultures displayed decreased chlorophyll *a* fluorescence, forward light scatter (a proxy for cell volume) and side light scatter (a proxy for granularity) relative to the inoculum culture (Caperon and Meyer 1972). The median normalized chlorophyll *a* fluorescence of cells was significantly anti-correlated to fCO_2 ($F_{1,10} = 4.09$, $p = 0.07$). The linear correlation was assessed on all data points, but for clarity CO_2 treatments were combined (Figure 5A). Median normalized forward and side scatter of cells were not significantly correlated to fCO_2 (Figure 5B,C). CO_2 treatment had a significant effect on chlorophyll *a* fluorescence ($p < 0.1$, two-way ANOVA), but acclimation condition and the interaction of the two factors were not significant.

Photosynthesis rates decreased with increasing CO_2 (Figure 6A) as expected for cells with reduced chlorophyll *a*. The inverse correlation of photosynthetic oxygen evolution and respiration rate with fCO_2 treatment were significant ($F_{1,8} = 11.17$, $p = 0.01$ for photosynthesis) ($F_{1,8} = 8.113$, $p = 0.02$ for respiration) (Figure 6B). We conducted a sensitivity test to assess the variability of photosynthesis and respiration rates with the choice of different parameters and assumptions (Fig. S1). The absolute values of photosynthetic oxygen evolution were sensitive to the choice of parameters, but the

inverse correlation was significant ($p < 0.05$) for all variations in the parameters tested. Respiration rates were more sensitive with some parameter choices resulting in non-significant linear correlations and negative respiration values, yet the trend of declining respiration with increasing fCO_2 was largely consistent. Due to the loss of one replicate each from low and medium CO_2 treatment, we could not assess the effect of acclimation, but we found that CO_2 treatment had a significant effect on photosynthesis and respiration rates ($p = 0.03$, $p= 0.04$ respectively ANOVA).

Discussion

The light reactions of photosynthesis and mitochondrial respiration are the main energy-producing processes in phytoplankton cells. We found a decrease in chlorophyll *a* and photosynthetic oxygen production in *T. pseudonana* under high CO_2 as well as declining respiration rates, indicating that the cells were decreasing energy production. The magnitude of the change in photosynthesis and respiration rates to fCO_2 treatment could not be determined in this study due to the sensitivity of our method to the choice of parameters. Importantly, a consistent negative correlation to fCO_2 was observed regardless of which parameters were chosen. This fits our hypothesis that under high CO_2, CCMs will be down-regulated leaving the cell with excess energy equivalents and, furthermore, cells would down-regulate energy production to prevent oxidative damage from excess energy equivalents. Our results agree with previous observations of changes in algal cell energy fluxes under elevated CO_2 including decreased photosynthesis (Rokitta and Rost 2012), increased photosystem II damage (McCarthy et al. 2012),

susceptibility to oxidative damage from UV light and decreased chlorophyll *a* per cell (Sobrino et al. 2008).

Our study demonstrates the utility of chemostat cultures in providing a stable acclimation environment for CO_2 studies. Nitrate limited chemostats rather than nutrient replete cultures provided a closer facsimile to conditions experienced by diatoms in the ocean. The chemostat cultures allowed the cells to be maintained under nitrate limitation with steady carbonate chemistry for 15-18 generations, to allow more consistent conditions for acclimation to the CO_2 treatment than would be possible with a batch culture. Using chemostat cultures that were not bubbled directly also made it possible to calculate budgets of carbon and nitrogen uptake and oxygen production by measuring concentrations and isotope composition (for O_2) from the inflow and outflow of the culturing vessel. Bubbling the culture vessel directly would have constantly replaced the dissolved gas and erased the signal of oxygen isotopes and carbon depletion caused by cell growth. The chemostat culturing method also allowed us to experiment with different acclimation conditions; the "long" acclimation utilized a more gradual increase in CO_2 (5-6 generations) while the "short" acclimation started at the target CO_2. While no incubation study can perfectly recreate *in situ* conditions, we believe our approach is advantageous for studying the acclimation of phytoplankton cultures in a tightly controlled and reproducible environment.

We hypothesized that the "long" acclimation where cultures were ramped up to the target CO_2 treatment would result in reduced cell oxidative stress. The ratio of DIC:DIN drawdown of the "long" acclimated cultures displayed no trend and was not significantly correlated with CO_2. However, the "short" acclimated cultures had increased

DIC:DIN drawdown that was significantly correlated with fCO_2. The increased DIC:DIN drawdown under short acclimation and high CO_2 was caused by decreasing DIN uptake and not increasing DIC fixation per cell (Figure 3). Given the observed decreases in chlorophyll *a* and photosynthesis per cell, the decrease in DIN uptake may reflect a decreased need for proteins in the plastid or photosynthetic apparatus of the cell. However, after a long acclimation, the cells exhibited no significant difference in DIC:DIN uptake from the low CO_2 condition. The trend of moderated physiological changes given a longer acclimation was also observed in chlorophyll *a* fluorescence per cell, photosynthesis and respiration rates in the high CO_2 treatment (S2), although to a lesser degree than the DIC:DIN uptake. The experimental design used here could not differentiate between the possibilities that the moderating effect was caused by (1) decreased cell oxidative stress response due to the gradual increase in CO_2, or (2) the result of phenotypic selection after more generations in culture, or (3) some combination of both effects.

We therefore used a differential growth rate model to test whether the observed change could be solely explained by phenotype selection. The long acclimated high CO_2 cultures grew under the target level of CO_2 for 10 days longer than the short acclimated cultures, which is equivalent to 15 additional generations. To test whether the cells could have been selected due to differential growth rate during these 10 days we performed a model experiment (Figure 7). In the model we assumed that daughter cells had the same DIC:DIN uptake as parent cells and that differences in growth rate and time in culture were the only factors that could act to shift the phenotype distribution from that observed with the short acclimation to that of the long acclimation (Figure 7A). We calculated

growth rates for the cells with respect to DIC:DIN (Figure 7B) that could explain the shift in distributions. The necessary growth rates span and even exceed the range of possible growth rates for *T. pseudonana* indicating that simply selecting phenotypes based on differential growth cannot fully explain the shift we observed.

The differences in cell physiology between short and long acclimations reflect physiological responses, including epigenetic changes or other gene regulatory responses. The differences were not likely evolutionary changes since our cultures were maintained for tens not thousands of generations (Collins and Bell 2004) additionally we ruled out phenotype selection based on growth rates alone. *T. pseudonana* possesses many of the required genes for epigenetic regulation, yet few studies have investigated the triggers of epigenetic control (Maumus et al. 2011). Cell signaling pathways for nutrient stress are starting to be identified in diatoms (Allen et al. 2006) and diatom regulatory networks are starting to be described in *T. pseudonana* (Ashworth et al. 2013), suggesting mechanisms for gene regulation that could help explain the physiological changes we observed.

Acclimation conditions, such as the number of generations algae are exposed to CO_2 treatment, vary widely between studies in ocean acidification research. The longest studies spanned 500-1000 generations (Collins and Bell 2004, Lohbeck et al. 2012) and the shortest studies spanned 3-5 generations (Trimborn et al. 2009). Tatters et al. (2012) found that the acclimation time was more significant than CO_2 treatment in determining dinoflagellate community composition. Culturing with nutrient limitation may also be important in simulating a more realistic algal physiology response to elevated CO_2 (King et al. 2011). The variation in acclimation and culturing conditions between previous experiments may partly explain the diverse and conflicting findings of those experiments.

Long acclimation experiments with slowly increasing CO_2 levels in the media can be logistically difficult to perform, but this research suggests they may be important for understanding how phytoplankton physiology will change as CO_2 levels slowly rise in the environment. Our results suggest the use of caution in designing and interpreting experiments with short acclimation times because the physiological changes may be dominated by cell oxidative stress responses rather than changes relevant to a specific environmental perturbation.

Acknowledgements

The authors gratefully acknowledge Michael O'Donnell for advice on the design of the CO_2 gas mixing system, Christopher Sabine for advice on the design of the chemostat outflow and carbonate chemistry, Jenny Lai for assistance in data collection, Mónica Orellana for helpful discussions and two anonymous reviewers for constructive criticism of the manuscript. We thank the National Science Foundation and the Gordon and Betty Moore Foundation for funding this research.

References

Abe, O. 2008. Isotope fractionation of molecular oxygen during adsorption / desorption by molecular sieve zeolite. *Rapid Communications in Mass Spectrometry*, 22:2510-4.

Allen, A. E., Vardi, A., & Bowler, C. 2006. An ecological and evolutionary context for integrated nitrogen metabolism and related signaling pathways in marine diatoms. *Current Opinion in Plant Biology*, 9(3): 264–73.

Ashworth, J., Coesel, S., Lee, A., Armbrust, E. V., Orellana, M. V, & Baliga, N. S. 2013. Genome-wide diel growth state transitions in the diatom Thalassiosira pseudonana. *Proceedings of the National Academy of Sciences of the United States of America*, *110*:7518–23.

Badger, M. R., Andrews, T. J., Whitney, S. M., Ludwig, M., Yellowlees, D. C., Leggat, W., & Price, G. D. 1998. The diversity and coevolution of Rubisco, plastids, pyrenoids, and chloroplast-based CO_2-concentrating mechanisms in algae. *Canadian Journal of Botany*, *76*:1052–1071.

Barkan, E., & Luz, B. 2005. High precision measurements of $^{17}O/^{16}O$ and $^{18}O/^{16}O$ ratios in H_2O. *Rapid Communications in Mass Spectrometry*, 19(24):3737-42.

Bauwe, H., Hagemann, M., & Fernie, A. R. 2010. Photorespiration: players, partners and origin. *Trends in Plant Science*, 15(6):330-6.

Berges, J. A., Franklin, D. J., & Harrison, P. J. 2001. Evolution of an artificial seawater medium: Improvements in enriched seawater, artificial water over the last two decades. *J. Phycol*, *37*:1138–45.

Berner, R. A. 2003. The long-term carbon cycle, fossil fuels and atmospheric composition. *Nature*, 426:323–6.

Borchard, C., Borges, A. V., Händel, N., & Engel, A. 2011. Biogeochemical response of Emiliania huxleyi (PML B92/11) to elevated CO_2 and temperature under phosphorous limitation: A chemostat study. *Journal of Experimental Marine Biology and Ecology*, 410:61–71.

Burkhardt, S., Amoroso, G., Riebesell, U., & Sultemeyer, D. 2001. CO_2 and HCO_3^- uptake in marine diatoms acclimated to different CO_2 concentrations. *Limnology and oceanography*, *46*(6):1378–1391.

Caperon, J., & Meyer, J. 1972. Nitrogen-limited growth of marine phytoplankton—I. changes in population characteristics with steady-state growth rate. *Deep Sea Research*, *19*(9):601–18.

Claquin, P., Kromkamp, J. C., & Martin-Jezequel, V. 2004. Relationship between photosynthetic metabolism and cell cycle in a synchronized culture of the marine alga Cylindrotheca fusiformis (*Bacillariophyceae*). *European Journal of Phycology*, *39*(1):33–41.

Collins, S., & Bell, G. 2004. Phenotypic consequences of 1,000 generations of selection at elevated CO_2 in a green alga. *Nature*, 431:566–9.

Crawfurd, K. J., Raven, J. A., Wheeler, G. L., Baxter, E. J., & Joint, I. 2011. The Response of Thalassiosira pseudonana to Long-Term Exposure to Increased CO_2 and Decreased pH. *PLoS ONE*, *6*(10):1–9.

Denman, K.L., Brasseur, G., Chidthaisong, A., Ciais, P., Cox, P.M., Dickinson, R.E., Hauglustaine, D., Heinze, C., Holland, E., Jacob, D., Lohmann, U., Ramachandran, S., da Silva Dias, P.L., Wofsy, S.C. & Zhang, X. 2007: Couplings Between Changes in the Climate System and Biogeochemistry. In: Climate Change 2007: The Physical Science Basis. Contribution of Working Group I to the Fourth Assessment Report of the Intergovernmental Panel on Climate Change [Solomon, S., Qin, D., Manning, M., Chen,

Z., Marquis, M., Averyt, K.B., Tignor, M. and Miller, H.L. (eds.)]. *Cambridge University Press*, Cambridge, United Kingdom and New York, NY, USA.

Dickson, A. G., Sabine, C. L., & Christian, J. R. 2007. Guide to Best Practices for Ocean CO_2 Measurements. *PICES Special Publication 3*.

Eisenstadt, D., Barkan, E., Luz, B., & Kaplan, A. 2010. Enrichment of oxygen heavy isotopes during photosynthesis in phytoplankton. *Photosynthesis Research*, 103:97–103.

Engel, a., Schulz, K. G., Riebesell, U., Bellerby, R., Delille, B., & Schartau, M. 2008. Effects of CO_2 on particle size distribution and phytoplankton abundance during a mesocosm bloom experiment (PeECE II). *Biogeosciences*, *5*(2):509–21.

Finkel, Z. V., Beardall, J., Flynn, K. J., Quigg, A., Rees, T. A. V., & Raven, J. A. 2009. Phytoplankton in a changing world: cell size and elemental stoichiometry. *Journal of Plankton Research*, *32*:119–37.

Hasle, G. R., & Heimdal, B. R. 1970. Some Species of the Centric Diatom Genus Thalassiosira Studied in the Light and Electron Microscopes. *Beihefte zur Nova Hedwigia*, 31:559–89.

Helman, Y., Barkan, E., Eisenstadt, D., Luz, B., & Kaplan, A. (2005). Fractionation of the Three Stable Oxygen Isotopes by Oxygen-Producing and Oxygen-Consuming Reactions in Photosynthetic Organisms. *Plant Physiology*, 138: 2292–8.

Hönisch, B., Ridgwell, a., Schmidt, D. N., Thomas, E., Gibbs, S. J., Sluijs, a., Zeebe, R., Kump, L., Martindale, R. C., Greene, S. E., Kiessling, W., Ries, J., Zachos, J. C., Royer,

D. L., Barker, S., Marchitto, T. M., Moyer, R., Pelejero, C., Ziveri, P., Foster, G. L. & Williams, B. 2012. The Geological Record of Ocean Acidification. *Science*, 335:1058–63.

Hopkinson, B. M., Dupont, C. L., Allen, A. E., & Morel, F. M. M. 2011. Efficiency of the CO2-concentrating mechanism of diatoms. *Proceedings of the National Academy of Sciences*, 108:3830–7.

Iglesias-Rodriguez, M. D., Halloran, P. R., Rickaby, R. E. M., Hall, I. R., Colmenero-Hidalgo, E., Gittins, J. R., Green, D. R. H., Tyrrell, T., Gibbs, S. J., von Dassow, P., Rehm, E., Armbrust, E. V. & Boessenkool, K. P. 2008. Phytoplankton calcification in a high-CO_2 world. *Science, 320*:336–40.

Kim, J.-M., Lee, K., Shin, K., Yang, E. J., Engel, A., Karl, D. M., & Kim, H.-C. 2011. Shifts in biogenic carbon flow from particulate to dissolved forms under high carbon dioxide and warm ocean conditions. *Geophysical Research Letters*, *38*: 1–5.

King, A. L., Sañudo-Wilhelmy, S. A., Leblanc, K., Hutchins, D. A., & Fu, F. 2011. CO_2 and vitamin B_{12} interactions determine bioactive trace metal requirements of a subarctic Pacific diatom. *The ISME journal*, 5:1388–96.

LaRoche, J., Rost, B., & Engel, A. 2010. Guide to best practices for ocean acidification research and data reporting, Part 2: Experimental design of perturbation experiments. *Publications of the Office of the European Union*, pp. 81–94.

Laws, E. a, Landry, M. R., Barber, R. T., Campbell, L., Dickson, M.-L., & Marra, J. 2000. Carbon cycling in primary production bottle incubations: inferences from grazing

experiments and photosynthetic studies using and in the Arabian Sea. *Deep Sea Research Part II: Topical Studies in Oceanography*, 47:1339–52.

Le Quéré, C., Andres, R. J., Boden, T., Conway, T., Houghton, R. a., House, J. I., Marland, G., Peters, G. P., van der Werf, G., Ahlström, A., Andrew, R. M., Bopp, L., Canadell, J. G., Ciais, P., Doney, S. C., Enright, C., Friedlingstein, P., Huntingford, C., Jain, A. K., Jourdain, C., Kato, E., Keeling, R. F., Klein Goldewijk, K., Levis, S., Levy, P., Lomas, M., Poulter, B., Raupach, M. R., Schwinger, J., Sitch, S., Stocker, B. D., Viovy, N., Zaehle, S. & Zeng, N. 2012. The global carbon budget 1959–2011. *Earth System Science Data Discussions*, 5:1107–57.

Lewis, E., & Wallace, D. 1998. *Program Developed for CO2 System Calculations*. Oak Ridge, Tennessee. Available at: http://cdiac.ornl.gov/oceans/co2rprt.html (last accessed 10 June, 2013)

Li, W., Gao, K., & Beardall, J. 2012. Interactive effects of ocean acidification and nitrogen-limitation on the diatom *Phaeodactylum tricornutum*. *PloS one*, *7*(12):1–8.

Lohbeck, K. T., Riebesell, U., & Reusch, T. B. H. 2012. Adaptive evolution of a key phytoplankton species to ocean acidification. *Nature Geoscience*, *5*:346–351.

Maumus, F., Rabinowicz, P., Bowler, C., & Rivarola, M. 2011. Stemming epigenetics in marine stramenopiles. *Current Genomics*, 12:357–70.

McCarthy, A., Rogers, S. P., Duffy, S. J., & Campbell, D. A. 2012. Elevated Carbon Dioxide Differentially Alters the Photophysiology of Thalassiosira Pseudonana (*Bacillariophyceae*) and Emiliania Huxleyi (*Haptophyta*). *J Phycol*, 48:635–646.

Meehl, G.A., Stocker, T.F., Collins, W.D., Friedlingstein, P., Gaye, A.T., Gregory, J.M., Kitoh, A., Knutti, R., Murphy, J.M., Noda, A., Raper, S.C.B., Watterson, I.G., Weaver, A.J. & Zhao, Z.-C. 2007: Global Climate Projections. In: Climate Change 2007: The Physical Science Basis. Contribution of Working Group I to the Fourth Assessment Report of the Intergovernmental Panel on Climate Change [Solomon, S., Qin, D., Manning, M., Chen, Z., Marquis, M., Averyt, K.B., Tignor, M. & Miller, H.L. (eds.)]. *Cambridge University Press*, Cambridge, United Kingdom and New York, NY, USA.

Moore, J. K., Doney, S. C., Glover, D. M., & Fung, I. Y. 2002. Iron cycling and nutrient-limitation patterns in surface waters of the World Ocean. *Deep Sea Research Part II: Topical Studies in Oceanography*, 49:463–507.

Nelson, D. M., Treguer, P., Brzezinski, M. A., Leynaert, A., & Queguiner, B. 1995. Production and dissolution of biogenic silica in the ocean: Revised global estimates, comparison with regional data and relationship to biogenic sedimentation. *Global Biogeochemical Cycle*, 9:359–72.

Quay, P.D., Emerson, S., Wilbur, D., Stump, C. and Knox, M. 1993. The $\delta^{18}O$ of dissolved O2 in the surface water of the subarctic Pacific: a Tracer of biological productivity, J. Geophys. Res. 98, 8447-8458.

Raven, J., & Johnston, A. M. 1991. Mechanisms of inorganic-carbon acquisition in marine phytoplankton and their implications for the use of other resources. *Limnology and Oceanography*, 36:1701–14.

Raven, J. A., Giordano, M., Beardall, J., & Maberly, S. C. 2012. Algal evolution in relation to atmospheric CO_2: carboxylases, carbon-concentrating mechanisms and carbon oxidation cycles. *Philosophical transactions of the Royal Society of London. Series B, Biological sciences*, 367:493–507.

Reinfelder, J. R. 2011. Carbon Concentrating Mechanisms in Eukaryotic Marine Phytoplankton. *Annual Review of Marine Science*, 3:291–315.

Riebesell, U., Schulz, K. G., Bellerby, R. G. J., Botros, M., Fritsche, P., Meyerhöfer, M., Neill, C., Nondal, G., Oschlies, A., Wohlers, J. & Zöllner, E. 2007. Enhanced biological carbon consumption in a high CO_2 ocean. *Nature*, 450:545–8.

Riebesell, U., Körtzinger, A., & Oschlies, A. 2009. Sensitivities of marine carbon fluxes to ocean change. *Proceedings of the National Academy of Sciences*, 106:20602–9.

Rokitta, S. D., & Rost, B. 2012. Effects of CO_2 and their modulation by light in the life-cycle stages of the coccolithophore *Emiliania huxleyi*. *Limnology and Oceanography*, 57:607–18.

Rouco, M., Branson, O., Lebrato, M., & Iglesias-Rodríguez, M. D. 2013. The effect of nitrate and phosphate availability on *Emiliania huxleyi* (NZEH) physiology under different CO_2 scenarios. *Frontiers in microbiology*, *4*:1–11.

Sabine, C. L., Feely, R. a, Gruber, N., Key, R. M., Lee, K., Bullister, J. L., Wanninkhof, R., Wong, C. S., Wallace, D. W. R., Tilbrook, B., Millero, F. J., Peng, T.-H., Kozyr, A., Ono, T. & Rios, A. F. 2004. The oceanic sink for anthropogenic CO2. *Science*, *305*:367–71.

Sarmiento, J. L., & Gruber, N. 2002. Sinks for Anthropogenic Carbon. *Physics Today*, 55:30-6.

Sobrino, C., Ward, M. L., & Neale, P. J. 2008. Acclimation to elevated carbon dioxide and ultraviolet radiation in the diatom Thalassiosira pseudonana: Effects on growth, photosynthesis, and spectral sensitivity of photoinhibition. *Limnology and Oceanography*, 53:494–505.

Takahashi, T., Sutherland, S. C., Wanninkhof, R., Sweeney, C., Feely, R. a., Chipman, D. W., Hales, B., Friederich, G., Chavez, F., Sabine, C., Watson, A., Bakker, D.C.E., Schuster, U., Metzl, N., Yoshikawa-Inoue, H., Ishii, M., Midorikawa, T., Nojiri, Y., Körtzinger, A., Steinhoff, T., Hoppema, M., Olafsson, J., Arnarson, T. S., Tilbrook, B., Johannessen, T., Olsen, A., Bellerby, R.,Wong, C.S., Delille, B., Bates, N.R. & de Baar, H.J.W. 2009. Climatological mean and decadal change in surface ocean pCO2, and net sea–air CO2 flux over the global oceans. *Deep Sea Research Part II: Topical Studies in Oceanography*, 56:554–577.

Tatters, A. O., Schnetzer, A., Fu, F., Lie, A. Y. A., Caron, D. A., & Hutchins, D. A. 2012. Short- Versus Long-Term Responses To Changing CO_2 in a Coastal Dinoflagellate Bloom: Implications for Interspecific Competitive Interactions and Community Structure. *Evolution*, 2:1–13.

Tatters, A. O., Roleda, M. Y., Schnetzer, A., Fu, F., Hurd, C. L., Boyd, P. W., … Hutchins, D. A. 2013. Short- and long-term conditioning of a temperate marine diatom community to acidification and warming. *Philosophical transactions of the Royal Society of London. Series B, Biological sciences*, *368*:1–14.

Trimborn, S., Wolf-Gladrow, D., Richter, K.-U., & Rost, B. 2009. The effect of pCO_2 on carbon acquisition and intracellular assimilation in four marine diatoms. *Journal of Experimental Marine Biology and Ecology*, 376:26–36.

Yang, G., & Gao, K. 2012. Physiological responses of the marine diatom *Thalassiosira pseudonana* to increased pCO_2 and seawater acidity. *Marine Environmental Research*, 79:142–51.

Table 1: Carbonate chemistry of chemostat cultures on sampling day. Carbonate chemistry parameters fugacity of CO_2 (fCO_2) and total alkalinity (TA) were calculated from measurements of pH and DIC using CO2SYS (Lewis and Wallace 1998). Values are averages of four biological replicates plus or minus the standard error.

CO_2 treatment	fCO_2 (µatm)	pH (total scale)	DIC (µmol kg^{-1})	TA (µmol kg^{-1})	Revelle factor
Low	333 ± 6	8.03 ± .01	1921 ±10	2215 ±17	10.11 ± 0.62
Medium	476 ± 18	7.90 ± .01	1991 ± 7	2222 ± 2	11.72 ± 0.35
High	816 ± 35	7.71 ± .02	2144 ±14	2299 ± 9	14.67 ± 0.23

Table 2: Corrected DIC uptake rates from sampling day. The DIC deficit in the chemostats compared to the media on sampling day (ΔDIC) was corrected by subtracting the measured DIC leak rate and a steady-state correction (see Methods). Values are averages of four biological replicates plus or minus the error. Errors were reported as the standard error of biological replicates or the propagated error of the measurement depending on which error was larger.

CO_2 treatment	ΔDIC (umoles kg^{-1} day^{-1})	DIC leak (umoles kg^{-1} day^{-1})	Steady-state correction (umoles kg^{-1} day^{-1})	Corrected ΔDIC (umoles kg^{-1} day^{-1})
Low	176 ± 6	16 ± 4	3 ± 3	158 ± 7
Medium	193 ± 8	43 ± 3	1 ± 3	149 ± 7
High	320 ± 22	144 ± 1	18 ± 10	157 ± 13

Figure 1: Experimental set-up of the chemostat cultures and CO_2 system. Samples were collected from syringe ports indicated by triangles. The dashed rectangle highlights the water trap drain on chemostat A; outflow from both chemostats flowed through a water trap drain to minimize gas exchange and bacterial contamination. The gas system mixed lab air with CO_2 using mass flow control (MFC) valves.

Figure 2: Nitrate-limited chemostats of *T. pseudonana* brought to steady state at three levels of CO_2: A) low (333 ± 6 μatm) B) medium (476 ± 18 μatm) C) high (816 ± 35 μatm). The asterisk (*) marks the last day of low CO_2 acclimation before the CO_2 was increased for medium (B) and high (C) CO_2 treatments in the long acclimated cultures. The error bars indicate the range of duplicate chemostat cultures. Note the change in Y-axis scale between panels.

Figure 3: Carbon and nitrogen uptake and production in steady state chemostat cultures at three fCO2 levels: low (333 ± 6 μatm); medium (476 ± 18 μatm); high (816 ± 35 μatm) indicated by white, grey and black bars respectively. Dissolved inorganic carbon (DIC) and dissolved inorganic nitrogen (DIN) uptake were calculated from depletion of inorganic carbon and nitrogen from the media, particulate organic carbon (POC) and particulate nitrogen (PON) production were calculated from the biomass composition and chemostat flow rates (see Methods). Error bars indicate SE of biological replicates (n=4).

Figure 4: Impact of fCO_2 treatment on Redfield ratio (DIC:DIN uptake). DIC:DIN ratios (unitless) of short acclimated cultures (black circles) are significantly correlated with

fCO_2 ($p < 0.01$), long acclimated cultures (gray squares) are not correlated. Error bars indicate propagated SE from measurement uncertainty.

Figure 5: Median chlorophyll *a* fluorescence (a), forward scatter (b) and side scatter (c) per cell normalized to median chlorophyll *a* fluorescence of exponentially growing cells. Error bars are SE (n=4).

Figure 6: Photosynthesis (a) and respiration rates (b) of chemostat cultures at low medium and high CO_2. The Mehler reaction and photorespiration are assumed to be negligible and the fractionation due to photosynthesis is assumed to be 1.0045 (see S1 for a sensitivity analysis of these parameters). Error bars are SE (n=3 for low and medium CO_2 and n=4 for high CO_2).

Figure 7: Model results of phenotype selection in the chemostats based on differential growth rates. Distributions of DIC:DIN uptake ratio (A) in short acclimated cultures (dashed line) and long acclimated cultures (solid line) for the high CO_2 chemostat, the arrow indicates the hypothesis that the short-acclimated culture distribution would shift to match the long-acclimated distribution after 10 days. Growth rate as a function of DIC:DIN uptake (B) was calculated to explain the shift in distributions from (A), light horizontal dashed lines indicate the range of possible growth rates of T. pseudonana at this light level.

S1: The sensitivity of photosynthesis (A) and respiration (B) rates to the choice of parameters in the calculation. Filled circles are solutions calculated assuming that the Mehler reaction and photorespiration each consume 20% and 5% of gross photosynthesis respectively. Unfilled circles are solutions assuming that the Mehler reaction and photosynthesis decline with increasing CO_2 from 20% and 5% respectively under low CO_2 to 0% under high CO_2. Filled triangles are solutions assuming that the Mehler reaction and photorespiration consume 0% of photosynthetic oxygen across all CO_2 treatments. Unfilled squares mark solutions calculated assuming that photosynthetic oxygen production does not fractionate $^{18}O/^{16}O$ (Guy et al. 1993) rather than the fractionation of 1.0045 used to calculate the other solutions (Eisenstadt et al. 2010). The lines associated with each set of points are the linear best fit, and p-values indicate the confidence in the correlation of the linear fit, error bars indicate the measurement uncertainty (±SD) as determined by Monte Carlo analysis.

S2: The effect of long and short acclimations on chlorophyll *a* content, photosynthesis and respiration rates versus fCO_2. Black circles represent short acclimation experiments; grey squares represent long acclimation experiments. Panels A, B, and C are normalized chlorophyll *a* fluorescence, photosynthesis and respiration rates respectively. The measurement uncertainty in median chlorophyll *a* fluorescence is very small due to a large sample size (>20,000 cells). The error bars on B and C indicate the measurement uncertainty (±SD) as determined by Monte Carlo analysis.

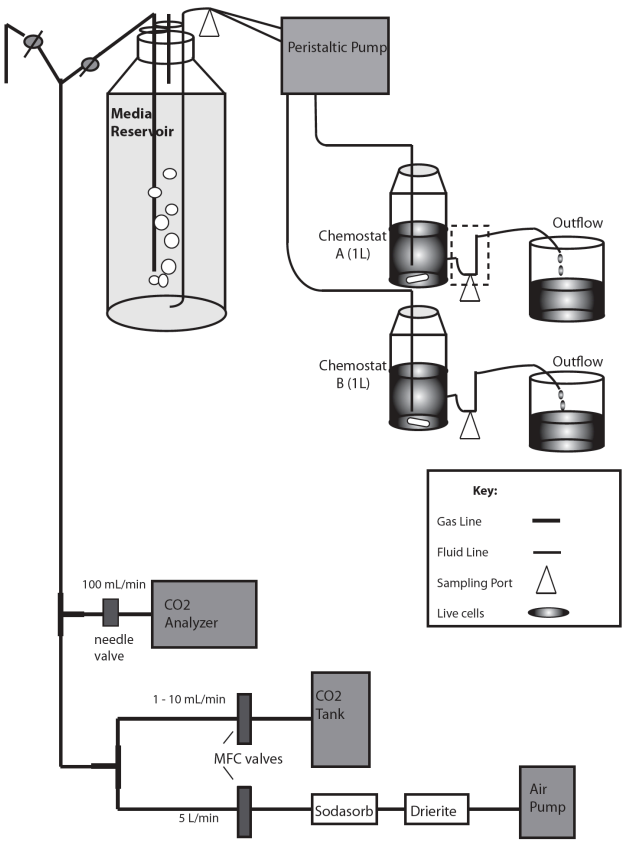
Peristaltic Pump
Media Reservoir
Chemostat A (1L)
Outflow
Chemostat B (1L)
Outflow
Key:
Gas Line
Fluid Line
Sampling Port
Live cells
100 mL/min
CO2 Analyzer
needle valve
1 - 10 mL/min
CO2 Tank
MFC valves
5 L/min
Sodasorb
Drierite
Air Pump

Figure 1

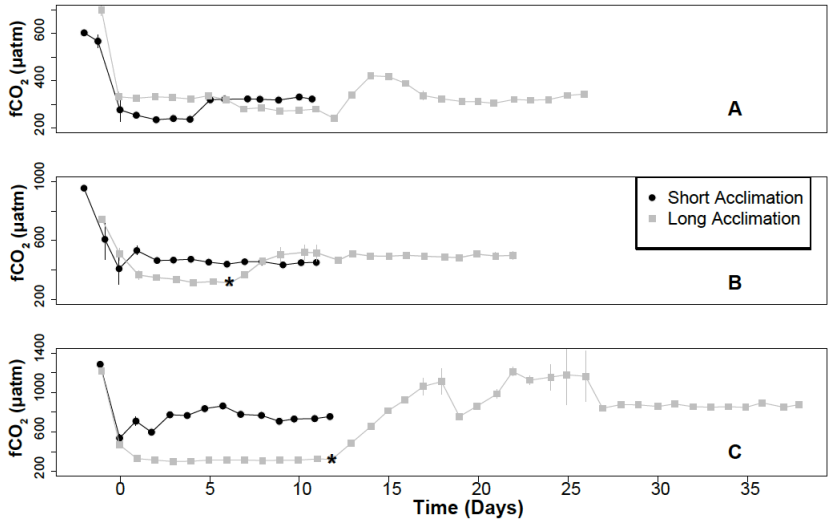
fCO2 (µatm)
200
400
600
A
fCO2 (µatm)
200
600
1000
Short Acclimation
Long Acclimation
B
fCO2 (µatm)
200
600
1000
1400
C
0
5
10
15
20
25
30
35
Time (Days)

Figure 2

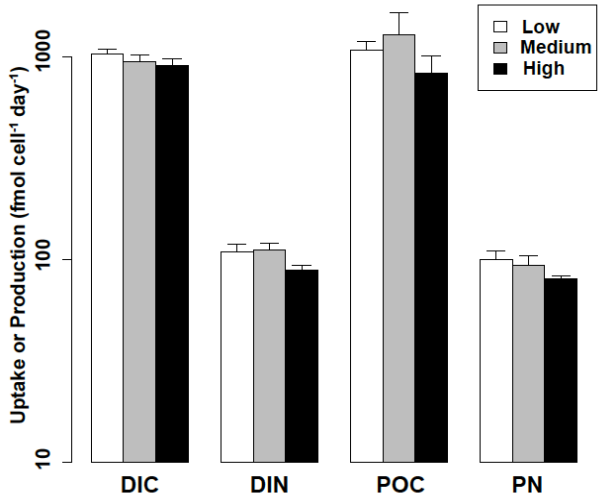
Low
Medium
High
Uptake or Production (fmol cell-1 day-1)
1000
100
10
DIC
DIN
POC
PN
Figure 3

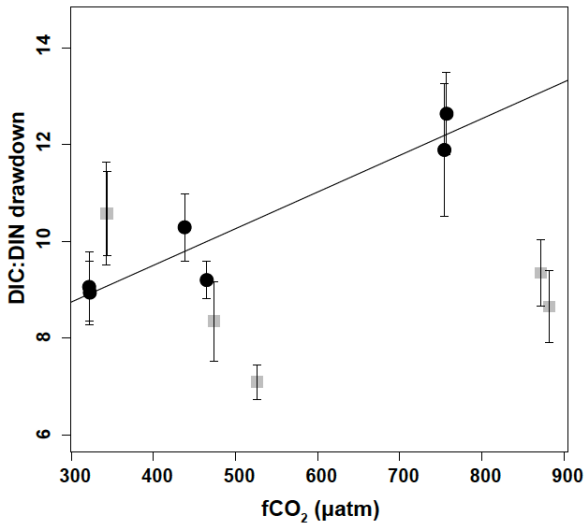
DIC:DIN drawdown
6
8
10
12
14
300
400
500
600
700
800
900
fCO2 (µatm)
Figure 4

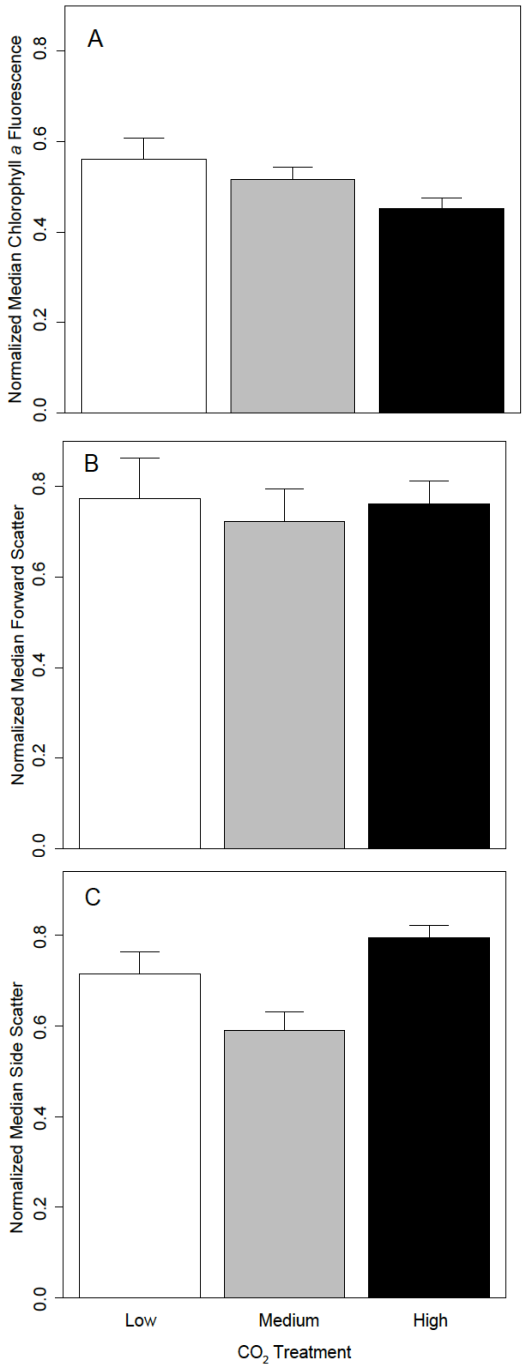
A
Normalized Median Chlorophyll a Fluorescence
0.0
0.2
0.4
0.6
0.8
B
Normalized Median Forward Scatter
0.0
0.2
0.4
0.6
0.8
C
Normalized Median Side Scatter
0.0
0.2
0.4
0.6
0.8
Low
Medium
High
CO2 Treatment

Figure 5

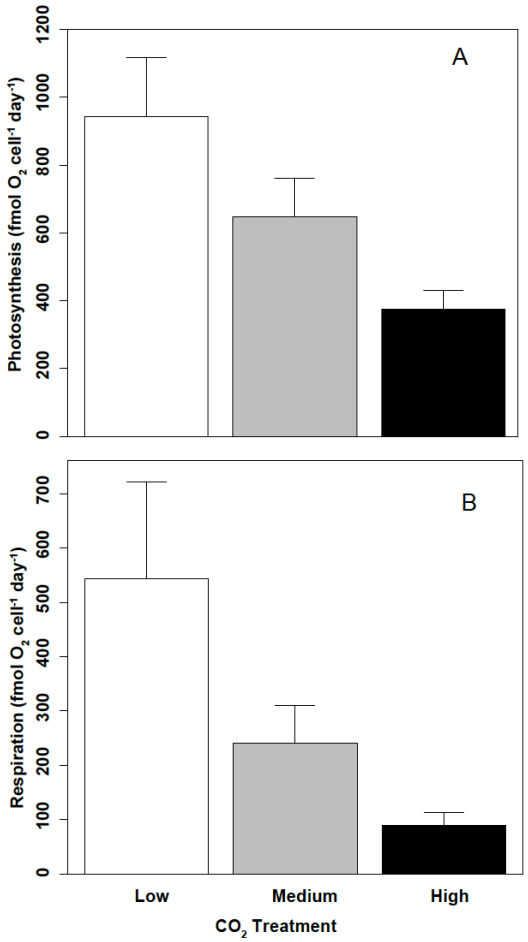
A
B
Photosynthesis (fmol O_2 cell^{-1} day^{-1})
Respiration (fmol O_2 cell^{-1} day^{-1})
0
200
400
600
800
1000
1200
100
300
500
700
Low
Medium
High
CO_2 Treatment

Figure 6

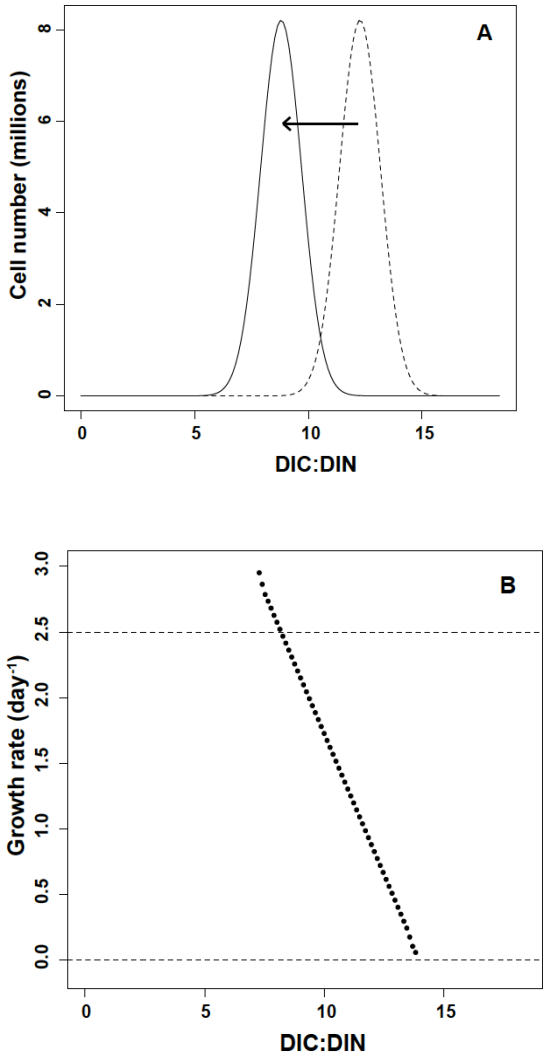
A
Cell number (millions)
0
2
4
6
8
0
5
10
15
DIC:DIN
B
Growth rate (day-1)
0.0
0.5
1.0
1.5
2.0
2.5
3.0
0
5
10
15
DIC:DIN

Figure 7

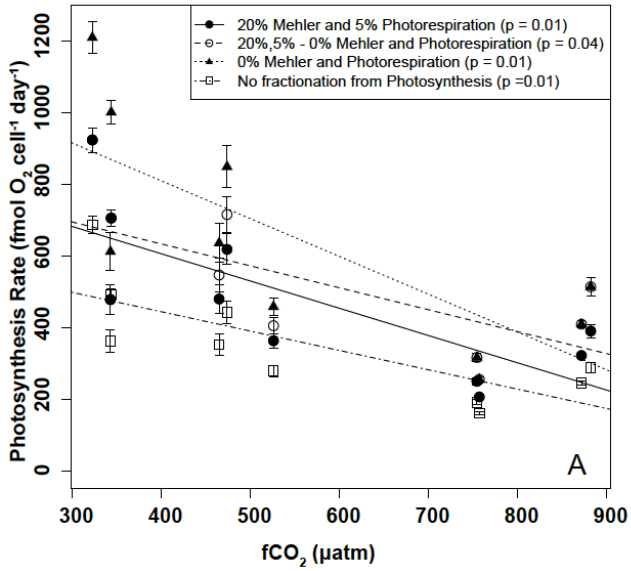
20% Mehler and 5% Photorespiration (p = 0.01)
20%,5% - 0% Mehler and Photorespiration (p = 0.04)
0% Mehler and Photorespiration (p = 0.01)
No fractionation from Photosynthesis (p =0.01)
Photosynthesis Rate (fmol O2 cell-1 day-1)
fCO2 (µatm)
A

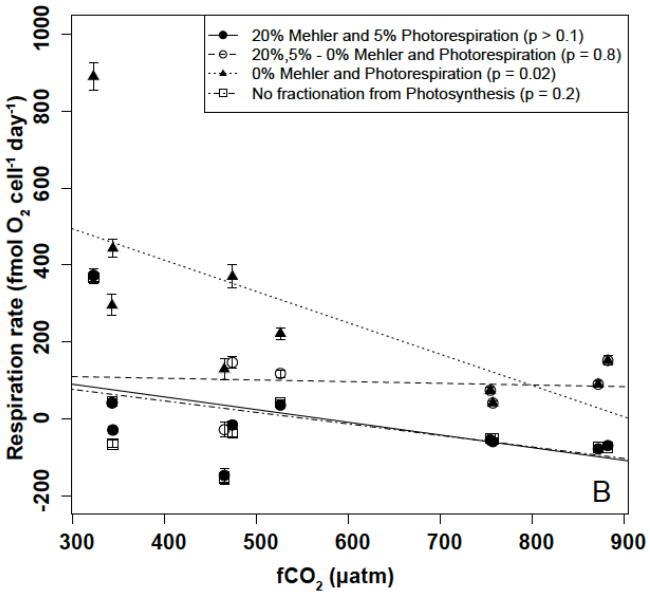
20% Mehler and 5% Photorespiration (p > 0.1)
20%,5% - 0% Mehler and Photorespiration (p = 0.8)
0% Mehler and Photorespiration (p = 0.02)
No fractionation from Photosynthesis (p = 0.2)
Respiration rate (fmol O2 cell-1 day-1)
fCO2 (µatm)
B

S1

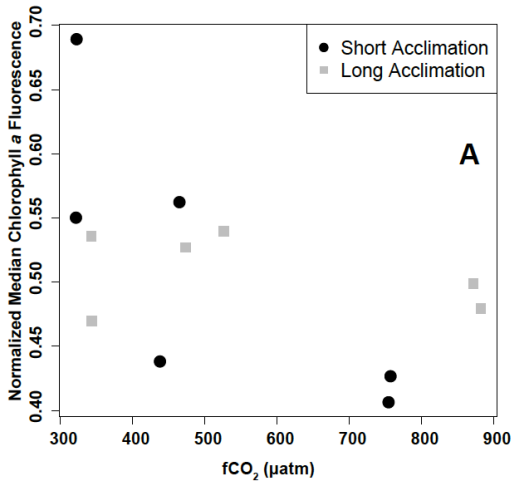
Short Acclimation
Long Acclimation
A
Normalized Median Chlorophyll a Fluorescence
0.40
0.45
0.50
0.55
0.60
0.65
0.70
300
400
500
600
700
800
900
fCO2 (µatm)

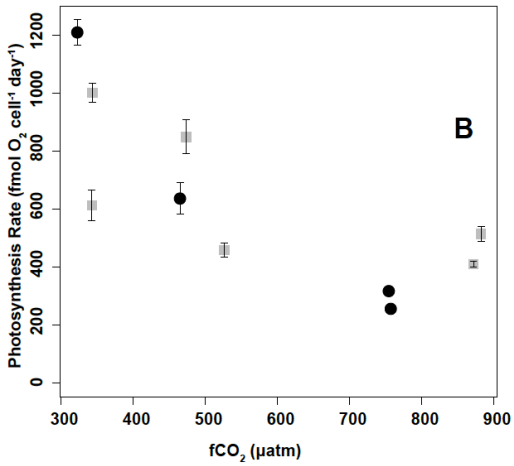
B
Photosynthesis Rate (fmol O2 cell-1 day-1)
0
200
400
600
800
1000
1200
300
400
500
600
700
800
900
fCO2 (µatm)

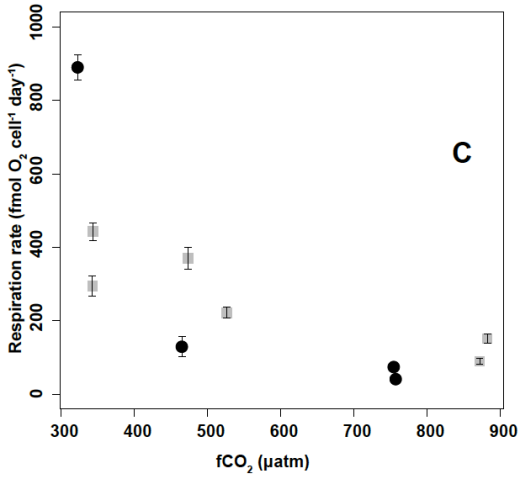
C
Respiration rate (fmol O2 cell-1 day-1)
0
200
400
600
800
1000
300
400
500
600
700
800
900
fCO2 (µatm)

S2

Chapter 2:

Title:

Diatom acclimation to elevated CO_2 via cAMP-signaling and coordinated gene expression

Authors: Gwenn M. M. Hennon[a]*, Justin Ashworth[b], Ryan D. Groussman[a], Chris Berthiaume[a], Rhonda L. Morales[a], Nitin S. Baliga[b], Mónica V. Orellana[b,c], E. V. Armbrust[a]*

Author Affiliations: [a]School of Oceanography, University of Washington, [b]Institute for Systems Biology, [c]Polar Science Center, University of Washington, Seattle WA

Contact Information: gwennm@uw.edu, armbrust@uw.edu

Reproduced with permission from Nature Publishing Group

Journal: Nature Climate Change

Hennon GMM, et al. (2015) Diatom acclimation to elevated CO2 via cAMP signalling and coordinated gene expression. *Nat Clim Chang* (June):1–6. Available at: http://www.nature.com/doifinder/10.1038/nclimate2683.

DOI: 10.1038/nclimate2683

Summary Paragraph

Diatoms are responsible for ~40% of marine primary productivity[1], fueling the oceanic carbon cycle and contributing to natural carbon sequestration in the deep ocean[2]. Diatoms rely on energetically expensive carbon concentrating mechanisms (CCMs) to fix carbon efficiently at modern levels of CO_2[3–5]. How diatoms may respond over the short and long-term to rising atmospheric CO_2 remains an open question. Here we use nitrate-limited chemostats to show that the model diatom *Thalassiosira pseudonana* rapidly responds to increasing CO_2 by differentially expressing gene clusters that regulate transcription and chromosome folding and subsequently reduces transcription of photosynthesis and respiration gene clusters under steady-state elevated CO_2. These results suggest that exposure to elevated CO_2 first causes a shift in regulation and then a metabolic rearrangement. Genes in one CO_2-responsive cluster included CCM and photorespiration genes that share a putative cyclic-AMP responsive *cis*-regulatory sequence, implying these genes are co-regulated in response to CO_2 with cAMP as an intermediate messenger. We verified cAMP-induced down-regulation of CCM gene δ-CA3 in nutrient-replete diatom cultures by inhibiting the hydrolysis of cAMP. These results indicate an important role for cAMP in down-regulating CCM and photorespiration genes under elevated CO_2 and provide insights into mechanisms of diatom acclimation in response to climate change.

Burning fossil fuels and land use change have accelerated CO_2 emissions to the atmosphere ~100 fold above natural levels[6]. About a third of anthropogenic emissions have been absorbed by the oceans[7,8], increasing dissolved CO_2 and reducing pH[9]. Despite these changes, CO_2 concentrations in surface waters remain below half-saturation for most forms of ribulose-1,5-bisphosphate carboxylase/oxygenase (Rubisco)[3], the central enzyme used to fix carbon. Consequently, marine phytoplankton, including diatoms, rely on carbon concentrating mechanisms (CCMs) to ensure adequate delivery of CO_2 to the Rubisco active site minimizing the competitive fixation of oxygen[3–5]. The required bicarbonate transporters and carbonic anhydrases of these CCMs concentrate CO_2 against a gradient, which is energetically costly[10]. Down-regulation of CCMs as part of acclimation to elevated CO_2 should result in energy savings to the diatom cell and metabolic rearrangement. Here we use nitrate-limited chemostats to simulate *in situ* nutrient limitation[11] while precisely controlling cell biomass and CO_2[12] allowing us to identify potential signaling pathways triggered either by an abrupt transition to increased CO_2 as might occur during coastal upwelling[13] or at steady-state exposure to elevated CO_2, including 800 μatm predicted for 2100[14] (Fig 1a,b).

Metabolic and regulatory genes were differentially impacted by changes in CO_2 (Fig. 1c). The initial response to an abrupt increase in CO_2 included up-regulation of genes required for transcriptional regulation and kinase activity (Fig. 1c), potentially reflecting CO_2-specific signaling mechanisms. Once steady-state conditions with elevated CO_2 were attained, genes required for energy producing metabolic pathways including oxidative phosphorylation, TCA cycle and photosynthesis were preferentially down-regulated as were genes involved in transcriptional regulation, ion transport, kinase

activity and protein degradation (Fig. 1c) suggesting a general reduction in metabolism under high CO_2. This corroborates our previous physiological measurements of decreased respiration and photosynthetic oxygen production under elevated CO_2 and nitrate-limitation[12]. A significant up-regulation of components of the ribosome under steady-state high CO_2 (Fig. 1c) may reflect either an increased capacity for protein synthesis or a high turnover of ribosomal proteins, while the down-regulation of the same gene category in transition suggests disparate modes of regulation between transition and steady-state exposure to elevated CO_2.

To identify potential linkages between an initial response and eventual metabolic rearrangements under steady state conditions, we identified groups of co-regulated genes based on unsupervised hierarchical clustering across a combined dataset of 98 RNA-seq and microarray data sets from a range of conditions[15–20] including our chemostat experiments. Of the 400 clusters of co-expressed genes, 160 displayed significant correlation to CO_2 partial pressure during transition or steady-state exposure (Spearman fdr < 0.0001) (Supplemental Table S1). The unsupervised clustering analysis yielded biologically-meaningful insights, grouping together functionally-related genes associated with energy metabolism including light harvesting, photosynthesis, and respiration (Fig. 2 a,b). These energy metabolism gene clusters were differentially expressed only after acclimation to steady-state elevated CO_2 along with other clusters containing genes implicated in cell signaling (Fig 2c,d), suggesting a suite of gene clusters are likely involved in diatom metabolic rearrangement. Expression of a gene cluster associated with regulation, structural maintenance of chromosomes (SMC), and transcription was correlated with CO_2 level during transition and steady-state exposure (Fig. 2e,f). This

cluster of regulatory genes, not previously connected to the diatom CO_2-response, could be involved in diatom cell regulation vital to sensing and acclimating to rising CO_2.

High external CO_2 is expected to reduce the need for the CCM as well as photorespiration, due to the competitive inhibition of Rubisco's oxygenase activity by CO_2[5]. Interestingly, a single cluster contained both putative CCM and photorespiration genes and was negatively correlated to CO_2 in both transition and steady-state experiments (Supplemental Table S1). This cluster further grouped into two distinct sub-clusters that displayed different expression patterns across the range of CO_2 concentrations examined in our experiments (Fig. 2e,f; Supplemental Figure S1). One sub-cluster included candidates for participation in the CCM such as the plastid-localized delta-carbonic anhydrase (δ-CA3)[21] and plastid-targeted transporters. The other sub-cluster included mitochondria-localized photorespiration genes necessary to recycle by-products of the oxygenase activity of Rubisco. The zeta-carbonic anhydrase ζ-CA1[21], also grouped with the photorespiration sub-cluster, is the only enzyme known to utilize cadmium as a cofactor[22] and is localized to the outer membrane space[21].

Given the strong correlation across our dataset of these sub-clusters of genes from separate pathways, we hypothesized they were regulated by a common mechanism. Genes in the CCM/photorespiration cluster all share a short upstream sequence (Supplemental Figure S1b), TGACGT, recently identified as a *cis*-regulatory sequence that down-regulates expression of the CO_2-responsive β-CA in the distantly-related diatom *Phaeodactylum tricornutum*[23]. Furthermore, two transcription factors, one in each sub-cluster, display close homology (Supplemental Figure S2) and are classified in the same phylogenetic group[24] as a cAMP-activated transcription factor in *P. tricornutum*

shown to bind the cis-regulatory element and to contribute to down-regulation of the β-CA gene in response to increased CO_2[23]. These lines of evidence suggest that the two transcription factors identified in the CCM/photorespiration cluster may function to down-regulate transcription of their own cluster by binding to the common upstream cis-regulatory region. This further implies that these transcription factors repress their own transcription, creating a negative feedback on the repression of this cluster, a feature common in biological systems[25].

We tested the proposed mechanism of cAMP-regulated gene expression with two indicator genes, carbonic anhydrase δ-CA3 and a putative transporter (pID 262258) that responded to CO_2 in both transition and steady state experiments with a large fold change (Supplemental Table S2). We grew *T. pseudonana* in nutrient-replete batch cultures and manipulated the CO_2 and the cellular level of cAMP by inhibiting its degradation with the phosphodiesterase inhibitor 3-isobutyl-1-methylxanthine (IBMX). The gene encoding δ-CA3 is a member of the CCM gene cluster and contains the upstream TGACGT motif. As predicted, transcript abundance for this gene was significantly ($p < 0.05$, two-way ANOVA) reduced by both high CO_2 and IBMX addition compared to low CO_2 (Fig. 3). The gene encoding the putative transporter lacks the cAMP-responsive motif. As predicted, transcript abundance for this gene was increased by elevated CO_2 but not significantly altered by the addition of IBMX ($p > 0.05$, t-test)(Fig. 3). These data suggest that gene expression patterns in response to CO_2 remain consistent independent of nitrate availability and that cAMP selectively down-regulates CO_2-responsive genes possessing the TGACGT motif.

Consistent with our data, mounting evidence[23,26] suggests that diatoms sense a change in external CO_2 concentrations, in part, through cAMP signaling. In other organisms[26,27] the activity of specific adenylyl cyclases are regulated by CO_2 or bicarbonate where increased CO_2 stimulates cyclase activity and results in enhanced production of cAMP[27]. This evidence suggests that increasing CO_2 concentrations promote a cyclase in *T. pseudonana* to increase production of cAMP, which in turn induces the CCM/photorespiration cluster transcription factors to bind to the TGACGT motif and repress transcription of CCM/photorespiration cluster genes, including their own transcription. The soluble cyclase (sol. CYCc, Fig. 4) and two membrane bound cyclases (CYCc, Fig. 2c,d, Fig.4) are among the candidates for sensing CO_2 in *T. pseudonana*. This mechanism is supported by the down-regulation of CCM/photorespiration cluster genes, including the transcription factors, by an increase in CO_2 and the down-regulation of δ-CA3 by addition of IBMX (Supplemental Table S2, Fig. 3).

Negative feedback mechanisms should result in a decreased repression of the CCM/photorespiration cluster genes over time unless changes in cAMP signaling or transcription factor regulation occur. We observed that cAMP metabolism genes were up-regulated at steady-state elevated CO_2 (Fig 4) including a phosphodiesterase, which degrades cAMP by hydrolysis, and two membrane bound cyclases (CYCc, Fig. 2c,d) that enhance production of cAMP. This indicates a change in cAMP metabolism at steady-state elevated CO_2, potentially altering how signals are propagated in cAMP responsive pathways, perhaps explaining why transcript abundance for the δ-CA3 gene is not further reduced under high CO_2 conditions in the presence of IBMX (Fig. 3). Likewise, the CCM sub-cluster transcription factor was no longer significantly repressed at steady-state

elevated CO_2 (Fig 4), potentially allowing it to attain sufficient abundance to maintain repression of the CCM and photorespiration pathway.

Placing the CCM and photorespiration gene clusters in the context of the diatom cell, we integrate predicted protein localization, gene transcription patterns, and metabolic pathways at steady-state elevated CO_2 (Fig 4) to gain insight into potential mechanisms of the diatom CO_2-response. A functioning diatom CCM must transport bicarbonate into the plastid to the stroma where it is converted to CO_2 by a carbonic anhydrase[10]. The CCM sub-cluster contains genes encoding plastid-localized membrane proteins including Bestrophin-like proteins, which are homologous to a family of gated anion-selective channels[28] permeable to bicarbonate [29] (Supplemental Table S2). These plastid-targeted proteins provide a feasible mechanism for bicarbonate transport to the stroma (Fig. 4), which has not yet been elucidated in diatoms. Once inside the plastid, bicarbonate can be converted to CO_2 by the stroma-localized[21], constitutively expressed α-CA1 (Fig. 4). Interestingly, this carbonic anhydrase is not down-regulated by CO_2, suggesting that unlike *P. tricornutum*[23], expression levels of a stromal-localized CA are not a point of CCM control in *T. pseudonana*. Another essential feature of efficient CCMs is to prevent the passive diffusion of enhanced CO_2 concentrations out of the cell in general or the plastid in particular[10]. The δ-CA3, localized to the plastid membrane space[21], and the ζ-CA1, localized to the outer membrane space[21], are well placed to serve this role by converting CO_2 into bicarbonate in the periplastid and periplasmic compartments, where it could be selectively transported back into the cytoplasm or stroma. That these genes are rapidly and sustainably down-regulated under elevated CO_2 suggests that preventing diffusive loss of CO_2 is tightly regulated as a point of control for the *T. pseudonana* CCM,

in strong agreement with physiology-based model predictions for an efficient diatom CCM[10].

Another feature of an efficient diatom CCM is active transport of bicarbonate from the external environment to the cell interior[10]; the SLC4-2 bicarbonate transporter is the most likely candidate as it is distantly related to a transporter demonstrated to serve this role in the diatom *P. tricornutum*[30] and the gene encoding this transporter was significantly down-regulated at steady-state high CO_2 (Fig. 4, Supplemental Table S2). Yet the SLC4-2 gene does not group with the CCM/photorespiration genes nor share the same upstream motif (Supplemental Table S1). Likewise, the plastid-localized phosphoglycolate phosphatase (PGP) gene, essential to the photorespiration pathway, was down-regulated at steady-state (Fig 4), but does not cluster with the mitochondrial photorespiration genes nor share the upstream region. cAMP-signal induced regulation cannot account for all the changes in gene expression since these and other known CCM and photorespiration genes were not down-regulated in lock-step (Fig 4) nor do they all contain the same upstream region. Transcription of a structural maintenance of chromosomes gene, co-expressed transcription factors, and histone proteins were significantly affected by an abrupt increase in CO_2 (Supplemental Table S2). These proteins function to modify chromosome structure to alter gene expression (Fig 4) and may explain shifts in CO_2 responsive genes not regulated by the cAMP-induced transcription factors.

The metabolic rearrangement we observed under steady-state elevated CO_2 and nitrate-limitation resulted from down-regulation of the energy consuming processes of CCM and photorespiration because cells were unable to increase growth rate due to

nitrate-limitation, a common limiting factor in the oceans[11]. Diatoms are also limited by other factors such as iron or light in vast regions of the ocean[11], and may display different metabolic rearrangements or growth rate enhancement in response to elevated CO_2 under these other conditions. Our analysis discovered genes that display CO_2 responses regardless of nitrogen status and provide insights into the mechanisms of CO_2 sensing, signaling, and metabolic rearrangement necessary to predict how diatoms will acclimate in future oceans. Our approach examining the behavior of co-expressed gene clusters in both transition and after steady-state acclimation is a powerful tool for beginning to untangle the mechanisms of sensing and responding to rising CO_2. Many of the CO_2-responsive genes identified by our clustering analysis were not previously connected to *T. pseudonana* CCM or CCM-regulation, allowing us to investigate new genes and mechanisms involved in regulating diatom physiology and biogeochemical cycles in the face of climate change.

Methods:

Chemostat cultures: For a full description of chemostat culturing methods see Hennon et al. (2014)[12]. Briefly, axenic *T. pseudonana* cells in four biological replicates (duplicate chemostats x 2 experimental runs) were acclimated to nitrate-limitation at 70% (1.5 day^{-1}) of max growth rate for >10 days (>15 generations) under continuous light of 80 µmol photons$\cdot m^{-2} \cdot s^{-1}$. Cell biomass was maintained at ~2 x 10^5 cells$\cdot mL^{-1}$ by 10 µM nitrate and carbonate chemistry stabilized to 300, 475 or 800 µatm CO_2, verified by calculating[31] fCO_2 from pH and DIC measurements. After steady-state acclimation, ~1 x 10^8 cells were harvested on 0.2 micron polycarbonate filters by gentle vacuum filtration and flash

frozen. Transition samples and carbonate chemistry were collected daily from chemostat cultures as CO_2 levels were increased from ~300-800 μatm at a rate ≤ 0.2 μatm·min^{-1} over four consecutive days (6 generations) after pre-acclimation to 300 μatm CO_2 and nitrate-limitation (Fig 1a,b). ~1.5x10^7 cells were harvested daily on 0.2 micron polycarbonate filters by gentle vacuum filtration and flash frozen.

Nutrient-replete cultures: Triplicate cultures of axenic *T. pseudonana* were grown in f/2 media under continuous illumination (300 μmol photons·m^{-2}·s^{-1}) at 20° C with constant aeration. Exponentially growing cultures were harvested with a cell density of ~4.2 x 10^5 cells mL^{-1} with 240 ± 19 μatm or 857 ± 54 μatm CO_2 verified by DIC and pH measurements (Supplemental Table S3). To inhibit the hydrolysis of cAMP 1.0 mM 3-isobutyl-1-methylxanthine (IBMX) was added to the cultures as described in previous work with the diatom *Phaeodactylum tricornutum*[32]. Before and after a 100 min exposure to 1.0 mM IBMX, ~4 x 10^8 cells were harvested by gentle vacuum filtration on a 0.8 μm filter and flash frozen for RT-qPCR analysis.

SOLiD libraries: A total of 28 barcoded transcriptome libraries were prepared from chemostat culture samples. RNA was extracted from filtered cells using the ToTALLY RNA kit (Life Technologies). Messenger RNA was selectively amplified using MessageAmp II aRNA Amplification kit (Life Technologies) and used to prepare SOLiD barcoded libraries (SOLiD Total RNA-seq kit, Life Technologies). Libraries were sequenced on a SOLiD 5500XL sequencer in two runs: one containing steady-state barcoded libraries and one containing transition barcoded libraries.

in silico read processing: Reads were quality controlled (using a cut-off of p =0.99 and minimum length =30), trimmed, and aligned to *T. pseudonana* gene models using the

Burrows-Wheeler Alignment tool and the SEAStAR tool (https://github.com/armbrustlab/SEAStAR). The aligned reads were counted for each gene model (Joint Genome Institute: thaps3 extended models) using the SEAStAR tool. RNA sequences and analysis products were deposited in NCBI's Gene Expression Omnibus and are accessible through GEO Series accession number GSE67971.

Gene Set Enrichment Analysis: Read counts from transition and steady-state transcriptomes were first normalized by the trimmed mean of M-values method (TMM: R package, edgeR)[33], then each gene was normalized to its own average expression level at low CO_2 (< 312 μatm for transition samples and < 350 μatm for steady-state samples) and log2 transformed. The normalized gene expression data was tested for correlation to CO_2 using the Spearman rank correlation test (cor.test, R stats). Genes with significant ($p < 0.05$) correlation to CO_2 in transition and steady-state transcriptomes were tested for significant gene set enrichment with the hypergeometric test (phyper, R stats) in categories defined by Kyoto Encyclopedia of Genes and Genomes (KEGG 58.1, June 1, 2011), Gene Ontology (GO 2009).

Gene clustering analysis: A dataset of 98 microarray and RNAseq samples representing ten experiments[15–20] was used to identify co-expressed gene clusters. All RNA-seq data were TMM normalized, and log2 ratios vs. triplicate control samples were combined with microarray log2 ratios. To estimate the co-expression of transcripts, Pearson pairwise correlation distances were computed across all samples following normalization such that all within-sample standard deviations were equal to one. Hierarchical clustering of these distances using Ward's method (fastcluster)[34] identified a hierarchy of co-expressed genes, from which 400 co-expressed groups were selected using arbitrary cut height.

Quality controls required a cluster to have at least 15 genes expressed with normalized mean square residual[35] < 0.6 across the CO_2 experiments and to be significantly correlated with CO_2 in transition or steady-state experiments (fdr < 0.0001) to be considered for further analysis. Multiscale bootstrap resampling was performed to estimate the significance and reproducibility of sub-clusters among this hierarchy. Candidate *cis*-regulatory regions were identified using MEME[36] from 0-800bp upstream of gene start sites, and TOMTOM[37] was used to assess similarity of candidate *cis*-regulatory motifs to previously characterized *cis*-regulatory elements.

Homology and alignments: Searches for homologous sequences were performed by Hidden Markov Model search tool (HMMsearch)[38] across the gene models. Multiple alignments were performed with MAFFT[39] and visualized in Jalview[40].

RT-qPCR: To quantify gene expression we used primers (Supplemental Table S4) to amplify genes for δ-CA3[41] and a putative transporter (pID 262258) from poly(A) selected RNA (MicroPoly(A)Purist kit, Life Technologies) on StepOnePlus Instrument with the Power SYBR Green RNA-to-CT 1-Step kit (Life Technologies). The gene copies were quantified in technical triplicate by a standard curve generated from the gene amplicon in a linearized 2.1 TOPO vector (Life Technologies) and normalized to mRNA in each sample. A two-way ANOVA (R stats, aov) was performed on δ-CA3 gene expression with a Tukey HSD *post hoc* test (R, stats, TukeyHSD) to determine significant differences between treatments and groups respectively. A student's t-test (R, stats, ttest) was performed on gene expression of the putative transporter at high CO_2 only since the low CO_2 gene expression was below the quantification limit of the standard curve.

References:

1. Nelson, D. M., Treguer, P., Brzezinski, M. A., Leynaert, A. & Queguiner, B. Production and dissolution of biogenic silica in the ocean: Revised global estimates, comparison with regional data and relationship to biogenic sedimentation. *Glob. Biogeochem. Cycle* **9,** 359–372 (1995).

2. Ducklow, H. W., Steinberg, D. K. & Buesseler, K. O. Upper Ocean Carbon Export and the Biological Pump. *Oceanography* **14,** 50–58 (2001).

3. Badger, M. R. *et al.* The diversity and coevolution of Rubisco, plastids, pyrenoids, and chloroplast-based CO_2-concentrating mechanisms in algae. *Can. J. Bot.* **76,** 1052–1071 (1998).

4. Giordano, M., Beardall, J. & Raven, J. A. CO_2 Concentrating Mechanisms in Algae: mechanisms, environmental modulation, and evolution. *Annu. Rev. Plant Biol.* **56,** 99–131 (2005).

5. Reinfelder, J. R. Carbon Concentrating Mechanisms in Eukaryotic Marine Phytoplankton. *Ann. Rev. Mar. Sci.* **3,** 291–315 (2011).

6. Berner, R. A. The long-term carbon cycle, fossil fuels and atmospheric composition. *Nature* **426,** 323–326 (2003).

7. Sabine, C. L. *et al.* The oceanic sink for anthropogenic CO_2. *Science* **305,** 367–71 (2004).

8. Le Quéré, C. *et al.* The global carbon budget 1959–2011. *Earth Syst. Sci. Data Discuss.* **5,** 1107–1157 (2012).

9. Caldeira, Ken, Wickett, M. Anthropogenic carbon and ocean pH. *Nature* **425,** 365–365 (2003).

10. Hopkinson, B. M., Dupont, C. L., Allen, A. E. & Morel, F. M. M. Efficiency of the CO_2-concentrating mechanism of diatoms. *Proc. Natl. Acad. Sci. U. S. A.* **108,** 3830–3837 (2011).

11. Moore, J. K., Doney, S. C., Glover, D. M. & Fung, I. Y. Iron cycling and nutrient-limitation patterns in surface waters of the World Ocean. *Deep Sea Res. Part II Top. Stud. Oceanogr.* **49,** 463–507 (2002).

12. Hennon, G. M. M., Quay, P., Morales, R. L., Swanson, L. M. & Armbrust, E. V. Acclimation conditions modify physiological response of the diatom *Thalassiosira pseudonana* to elevated CO_2 concentrations in a nitrate-limited chemostat. *J. Phycol.* **253,** 243–253 (2014).

13. Feely, R. a, Sabine, C. L., Hernandez-Ayon, J. M., Ianson, D. & Hales, B. Evidence for upwelling of corrosive 'acidified' water onto the continental shelf. *Science* **320,** 1490–2 (2008).

14. Ciais, P. *et al. Carbon and Other Biogeochemical Cycles. In: Climate Change 2013: The Physical Science Basis*. (2013).

15. Mock, T. *et al.* Whole-genome expression profiling of the marine diatom *Thalassiosira pseudonana* identifies genes involved in silicon bioprocesses. *Proc. Natl. Acad. Sci. U. S. A.* **105,** 1579–84 (2008).

16. Carvalho, R. N., Bopp, S. K. & Lettieri, T. Transcriptomics responses in marine diatom *Thalassiosira pseudonana* exposed to the polycyclic aromatic hydrocarbon benzo[a]pyrene. *PLoS One* **6,** e26985 (2011).

17. Thamatrakoln, K., Korenovska, O., Niheu, a K. & Bidle, K. D. Whole-genome expression analysis reveals a role for death-related genes in stress acclimation of the diatom *Thalassiosira pseudonana*. *Environ. Microbiol.* **14,** 67–81 (2012).

18. Shrestha, R. P. *et al.* Whole transcriptome analysis of the silicon response of the diatom *Thalassiosira pseudonana*. *BMC Genomics* **13,** 499 (2012).

19. Ashworth, J. *et al.* Genome-wide diel growth state transitions in the diatom *Thalassiosira pseudonana*. *Proc. Natl. Acad. Sci. U. S. A.* **110,** 7518–23 (2013).

20. Bender, S. J., Durkin, C. a., Berthiaume, C. T., Morales, R. L. & Armbrust, E. V. Transcriptional responses of three model diatoms to nitrate limitation of growth. *Front. Mar. Sci.* **1,** 1–15 (2014).

21. Samukawa, M., Shen, C., Hopkinson, B. M. & Matsuda, Y. Localization of putative carbonic anhydrases in the marine diatom, *Thalassiosira pseudonana*. *Photosynth. Res.* **121,** 235–249 (2014).

22. Xu, Y., Feng, L., Jeffrey, P. D., Shi, Y. & Morel, F. M. M. Structure and metal exchange in the cadmium carbonic anhydrase of marine diatoms. *Nature* **452,** 56–61 (2008).

23. Ohno, N. *et al.* CO_2-cAMP-responsive cis-elements targeted by a transcription factor with CREB/ATF-like basic zipper domain in the marine diatom *Phaeodactylum tricornutum*. *Plant Physiol.* **158,** 499–513 (2012).

24. Rayko, E., Maumus, F., Maheswari, U., Jabbari, K. & Bowler, C. Transcription factor families inferred from genome sequences of photosynthetic stramenopiles. *New Phytol.* **188,** 52–66 (2010).

25. Krishna, S., Andersson, A. M. C., Semsey, S. & Sneppen, K. Structure and function of negative feedback loops at the interface of genetic and metabolic networks. *Nucleic Acids Res.* **34,** 2455–62 (2006).

26. Matsuda, Y., Nakajima, K. & Tachibana, M. Recent progresses on the genetic basis of the regulation of CO_2 acquisition systems in response to CO_2 concentration. *Photosynth. Res.* **109,** 191–203 (2011).

27. Hammer, A., Hodgson, D. R. W. & Cann, M. J. Regulation of prokaryotic adenylyl cyclases by CO_2. *Biochem. J.* **396,** 215–8 (2006).

28. Dickson, V. K., Pedi, L. & Long, S. B. Structure and insights into the function of a Ca^{2+}-activated Cl^- channel. *Nature* (2014). doi:10.1038/nature13913

29. Qu, Z. & Hartzell, H. Bestrophin Cl^- channels are highly permeable to HCO_3^-. *Am. J. Cell Physiol.* **294,** 1371–1377 (2008).

30. Nakajima, K., Tanaka, A. & Matsuda, Y. SLC4 family transporters in a marine diatom directly pump bicarbonate from seawater. *Proc. Natl. Acad. Sci. U. S. A.* **110,** 1767–72 (2013).

31. Lewis, E. & Wallace, D. *Program Developed for CO2 System Calculations*. (1998). at <http://cdiac.ornl.gov/oceans/co2rprt.html>

32. Harada, H., Nakajima, K., Sakaue, K. & Matsuda, Y. CO2 sensing at ocean surface mediated by cAMP in a marine diatom. *Plant Physiol.* **142,** 1318–28 (2006).

33. Robinson, M. D. & Oshlack, A. A scaling normalization method for differential expression analysis of RNA-seq data. *Genome Biol.* **11,** R25 (2010).

34. Mullner, D. fastcluster : Fast Hierarchical , Agglomerative Clustering Routines for R and Python. *J. Stat. Softw.* **53,** 1–18 (2013).

35. Reiss, D. J., Baliga, N. S. & Bonneau, R. Integrated biclustering of heterogeneous genome-wide datasets for the inference of global regulatory networks. *BMC Bioinformatics* **7,** 280 (2006).

36. Bailey, T. & Elkan, C. *Fitting a mixture model by expectation maximization to discover motifs in biopolymers*. (1994). at <http://biofactory.org/sites/default/files/presentations/motif.pdf>

37. Gupta, S., Stamatoyannopoulos, J. a, Bailey, T. L. & Noble, W. S. Quantifying similarity between motifs. *Genome Biol.* **8,** R24 (2007).

38. Eddy, S. R. Accelerated profile HMM searches. *PLoS Comput. Biol.* **7,** (2011).

39. Katoh, K. & Standley, D. M. MAFFT multiple sequence alignment software version 7: Improvements in performance and usability. *Mol. Biol. Evol.* **30,** 772–780 (2013).

40. Waterhouse, A. M., Procter, J. B., Martin, D. M. a, Clamp, M. & Barton, G. J. Jalview Version 2-A multiple sequence alignment editor and analysis workbench. *Bioinformatics* **25,** 1189–1191 (2009).

41. Crawfurd, K. J., Raven, J. a., Wheeler, G. L., Baxter, E. J. & Joint, I. The Response of Thalassiosira pseudonana to Long-Term Exposure to Increased CO2 and Decreased pH. *PLoS One* **6,** 1–9 (2011).

Correspondence and requests for materials should be addressed to Gwenn Hennon (gwennm@uw.edu) or E.V. Armbrust (armbrust@uw.edu)

Acknowledgements: National Science foundation (Grants OCB-0928561 and MCB-1316206 to M.V.O. and N.S.B.; OCE- 0927238 to E.V.A.), Gordon and Betty Moore Foundation (Grant 537.01 to E. V. A.). We thank Dr. S. Amin for comments on the manuscript and Dr. B. Durham for advice on RT-qPCR.

Author Contributions: RNA sample preparation, sequencing and RT-qPCR: GMMH, RLM, RDG; bioinformatics and statistics: GMMH, JA, CB; experimental design: GMMH, JA, MO, NSB, EVA; manuscript preparation: GMMH, JA, RDG, EVA. All authors contributed to discussion of results and comments on the manuscript.

Competing Financial Interests:

The authors declare no competing financial interests.

Figure Legends:

Figure 1: Gene set enrichment in transition and steady-state nitrate-limited cultures. *Thalassiosira pseudonana* exposed to (a) transition from low to high CO_2 over four days or (b) steady-state acclimation to low, medium or high CO_2 (lighter and darker shades respectively) (mean ± SD, n=4). Genes significantly (c) positively (red) or negatively

(blue) correlated with CO_2 (Spearman rank correlation $p < 0.05$) formed gene sets categorized by KEGG pathway and GO term. The ratio of gene number to expected value (fold enrichment) in each category are plotted on the y-axis; dashed line indicates expected value and asterisk indicates significant enrichment in positively or negatively correlated gene sets (hypergeometric test $p < 0.05$).

Figure 2: Clusters of co-expressed genes versus CO_2 in transition and steady-state experiments. Fold change (mean ± 2SE) of clusters of co-expressed genes normalized to expression under low CO_2. Gene clusters involved in energy-producing metabolic pathways (a,b), and sensing and intracellular signal propagation (c,d). A regulatory cluster and photorespiration and CCM subclusters (e,f). Expression of selected individual genes are indicated with solid lines representing smoothed mean expression and points representing single transcriptome measurements relative to low CO_2. Abbreviations for genes are: Cytochrom_c1= Cytochrome C1 oxidase, Photosystem II subunit: PsbU, CYCc= adenylate/guanylate cyclase, PDE= phosphodiesterase, Rab= Rab-like small GTPase, SMC= structural maintenance of chromosomes protein, CA= carbonic anhydrase, GDCT= glycine decarboxylase T protein.

Figure 3: cAMP and CO_2 dependence of gene expression in nutrient-replete cultures. Transcript abundance normalized to messenger RNA (mean ± 1.96 SE: 95% CI, n=3) of genes encoding carbonic anhydrase δ-CA3 (grey), and a putative transport protein (white) pID 262258, in nutrient-replete cultures. *T. pseudonana* cells were exposed to low (240 ± 15 μatm) or high (857 ± 54 μatm) CO_2, with or without 1.0 mM of the phosphodiesterase inhibitor 3-isobutyl-1-methylxanthine (IBMX) used to elevate cellular cAMP concentrations. Dashed line indicates the quantification limit of transcript abundance by RT-qPCR and letters indicate significant differences among treatments for δ-CA3 gene expression ($p < 0.05$, two-way ANOVA and Tukey HSD).

Figure 4: Model of cell signaling and metabolite fluxes in *T. pseudonana* after acclimation to high CO_2. Gene expression changes relative to low CO_2 in high CO_2 steady-state experiments indicated by the heat map (log_2 Fold Change) overlaid on a model of diatom CO_2-responsive signaling and metabolic pathways. Membership in the CCM sub-cluster and photorespiration cluster indicated by * and † respectively with bold borders. Solid arrows indicate reactions and dashed arrows indicate regulatory relationships. Abbreviations: SPT/AGT= serine-pyruvate/aspartate aminotransferase, TF= transcription factor, SHMT= serine-glycine hydroxymethyltransferase, GDC(P/T)= glycine decarboxylase (P/T) protein, GOX= glycolate oxidase, MFS= major facilitator superfamily, Bestrophin= bestrophin superfamily transporter, PGP= phospho-glycolate phosphatase, SLC4= solute carrier family 4 bicarbonate transporter, others as in Fig. 2.

Supplemental Table S1: Gene cluster assignment and correlation with CO_2. Gene clusters described in Figure 2 are highlighted and described according to the figure legend. Normalized mean square residuals (Reiss et al. 2006) were calculated for gene expression within each cluster across all samples and CO_2 experiments alone (this study). Each cluster was tested for spearman rank correlation with CO_2 partial pressure across all genes in the cluster for both transition and steady-state

experiments and the p-values were corrected for false discovery rate (fdr). Clusters that were significantly correlated with CO_2 (fdr < 0.0001) are indicated (1=True). The number of proteins as well as JGI protein IDs and annotations are listed for each cluster. Format: Excel Table, size: 235 kb

Supplemental Table S2: Differential expression, cell localization and literature support for select CO_2-responsive genes. Selected CO_2-responsive genes are shown with differential expression statistics (R package, edgeR): log_2 Fold Change under high CO_2 in transition and steady-state experiments, log_2 Counts per million (gene abundance), likelihood ratio (LR statistic), p-value, and false discovery rate corrected p-value (fdr). Predicted and confirmed localization, and the presence of transmembrane domains are listed for each gene along with literature references. Format: Excel Table, size: 70 kb

Supplemental Table S3: Carbonate chemistry of nutrient-replete culture experiment. The mean (± SD, n=3) pH measured by spectroscopy with m-cresol purple dye and dissolved inorganic carbon (DIC) measured by AS-C3 DIC analyzer (Apollo SciTech Inc., Bogart, GA, USA) for low and high CO_2 treatments were used to calculate the partial pressure of CO_2 (pCO_2) and total alkalinity (TA) in CO2SYS software (Lewis and Wallace, 1998). Format: Excel Table, size: 9 kb

Supplemental Table S4: Primers for RT-qPCR. Gene name and JGI protein identifier for both genes used in RT-qPCR with primer sequences, amplicon size, melting temperature, genome location and citation. Format: Excel Table, size: 27 kb

Supplemental Figure S1: Cluster of co-expressed CCM and photorespiration genes. (a) Heat map of relative gene expression from a cluster containing photorespiration and putative CCM genes across 98 different RNA-seq and microarray measurements categorized by experimental treatment. The dendrogram indicates expression similarity between genes according to the cluster analysis; the sub-cluster in blue includes putative CCM genes and the sub-cluster in grey includes photorespiration genes (bold). Carbonic anhydrases (CA) in italicized bold. * indicates plastid-targeted proteins. Labels include annotation and JGI protein ID. Approximately unbiased (au) bootstrap values indicated at the nodes. (b) Potential *cis*-regulatory motif in the upstream region of all 21 genes in the photorespiration/CCM cluster (MEME, E-value 1.0e-005). Abbreviations: SPT/AGT= serine-pyruvate/aspartate aminotransferase, Thr-dehyd= threonine dehydratase, TF= transcription factor, SHMT= serine-glycine hydroxymethyltransferase, GDC(P/T)= glycine decarboxylase (P/T) protein, MAO= malic enzyme, Radical_SAM = radical S-adenosylmethionine protein family, Orn-CydA= ornithine cyclodeaminase, GOX= glycolate oxidase, MFS= major facilitator superfamily, Bestrophin= bestrophin superfamily transporter. Format: PDF, size: 344 kb

Supplemental Figure S2: Multiple alignment showing a conserved region of CCM/photorespiration transcription factors with previously characterized transcription factors. Amino acid alignment of transcription factors with colors indicating the dominant amino acid chemical properties (Clustal X coloring). Bars

below indicate amino acid conservation, alignment quality score and the consensus amino acid sequence (Jalview). The reference sequences are transcription factors in *Phaeodactyulm tricornutum* and *Homo sapiens* which have been experimentally verified to bind the motif TGACGT (Ohno et al. 2012). Format: PDF, size: 50 kb

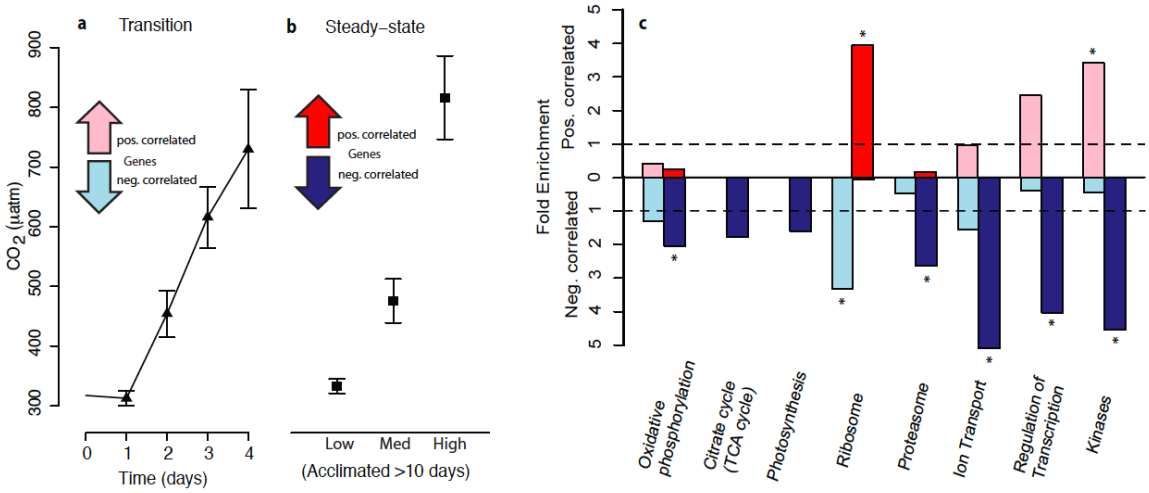
a
Transition
b
Steady–state
pos. correlated
Genes
neg. correlated
CO_2 (µatm)
300
400
500
600
700
800
900
0
1
2
3
4
Time (days)
Low
Med
High
(Acclimated >10 days)
c
Fold Enrichment
Pos. correlated
Neg. correlated
Oxidative phosphorylation
Citrate cycle (TCA cycle)
Photosynthesis
Ribosome
Proteasome
Ion Transport
Regulation of Transcription
Kinases

Figure 1

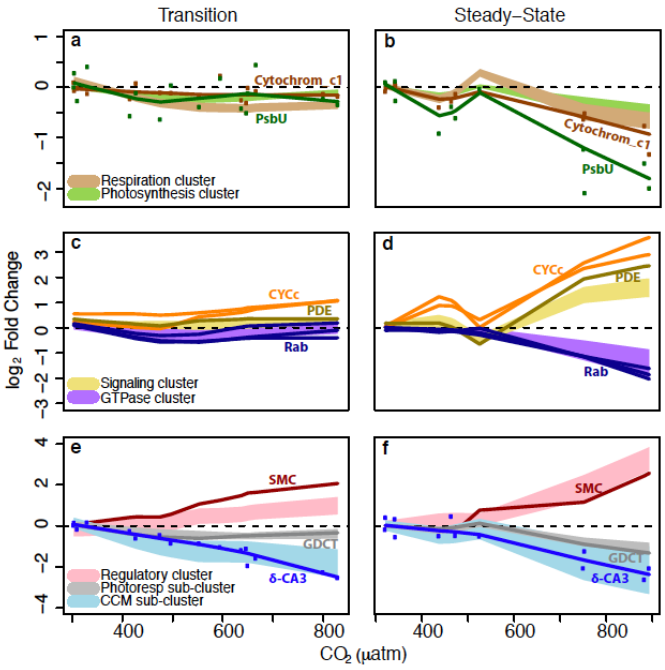
Transition
Steady–State
a
b
c
d
e
f
Cytochrom_c1
PsbU
Respiration cluster
Photosynthesis cluster
CYCc
PDE
Rab
Signaling cluster
GTPase cluster
SMC
GDCT
δ-CA3
Regulatory cluster
Photoresp sub-cluster
CCM sub-cluster
log2 Fold Change
CO2 (µatm)

Figure 2

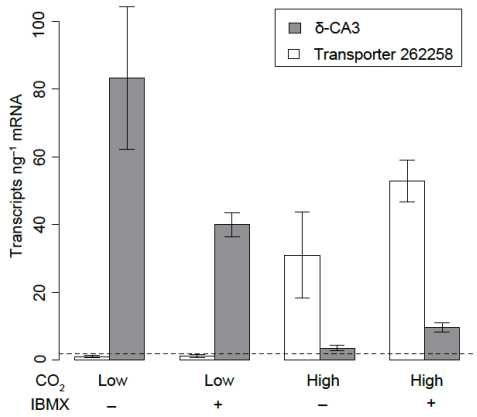
δ-CA3
Transporter 262258
Transcripts ng⁻¹ mRNA
0
20
40
60
80
100
CO2
IBMX
Low
Low
High
High
–
+
–
+

Figure 3

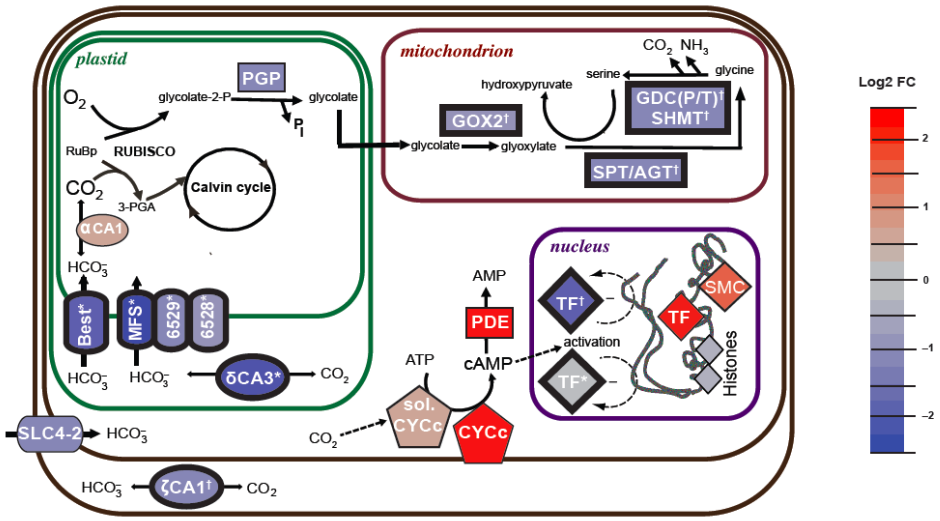
plastid
PGP
O2
glycolate-2-P
glycolate
Pi
RuBp
RUBISCO
CO2
3-PGA
Calvin cycle
αCA1†
HCO3-
Best*
MFS*
6529*
6528*
HCO3-
HCO3-
δCA3*
CO2
SLC4-2
HCO3-
HCO3-
ζCA1†
CO2
mitochondrion
CO2 NH3
serine
glycine
hydroxypyruvate
GOX2†
GDC(P/T)†
SHMT†
glycolate
glyoxylate
SPT/AGT†
AMP
PDE
ATP
cAMP
sol. CYCc
CYCc
CO2
nucleus
TF†
TF*
activation
TF
SMC
Histones
Log2 FC
2
1
0
−1
−2

Figure 4

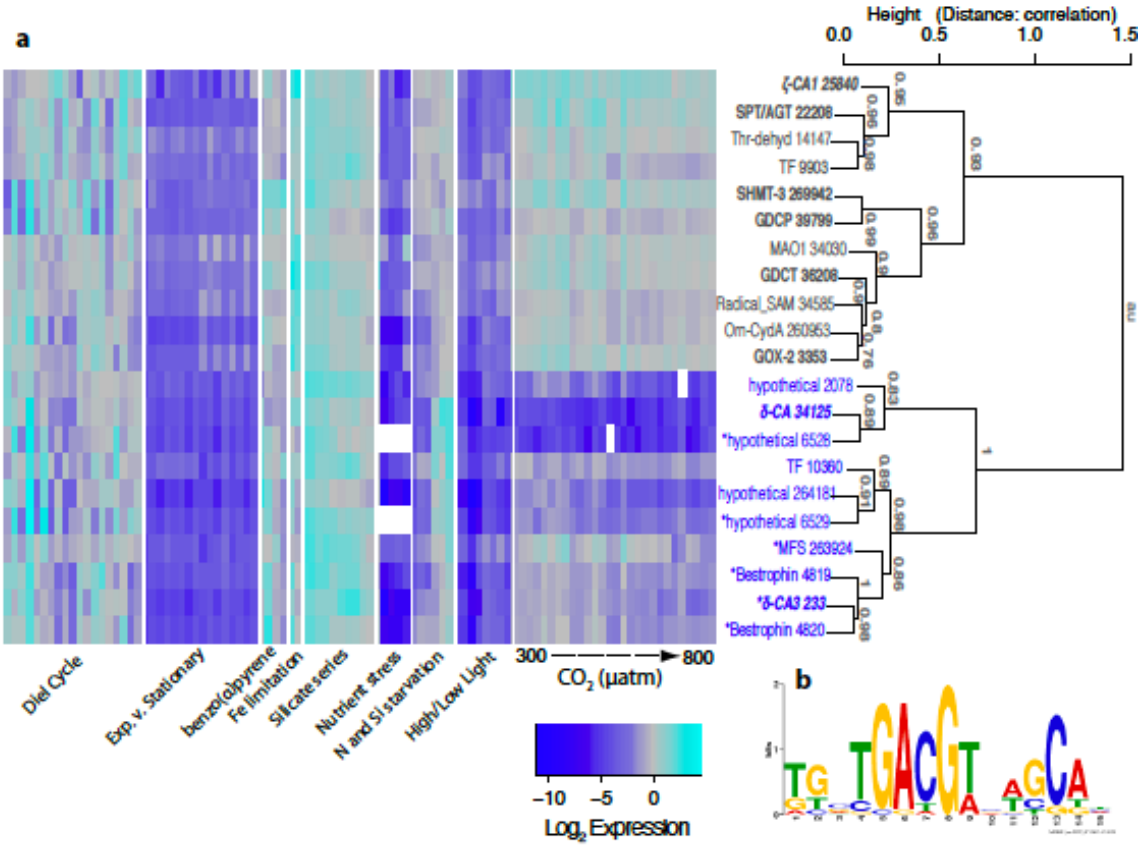

Supplemental Figure 1

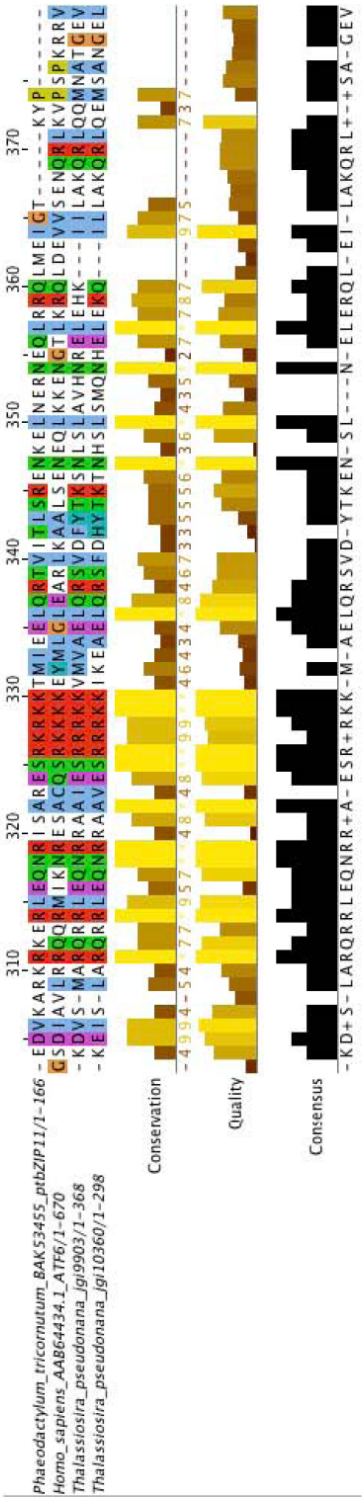

Supplemental Figure 2

Chapter 3:

Title: *In situ* division rates of *Prochlorococcus* suggest a shift from ammonium to nitrate utilizing ecotypes from the tropical to subtropical Atlantic

Authors: Gwenn M. M. Hennon[1], Evan Howard[2], Francois Ribalet[1], E. V. Armbrust[1]

Affliliations: 1. School of Oceanography University of Washington, Seattle WA, USA; 2. Woods Hole Oceanographic Institution, Woods Hole MA, USA

Corresponding author: armbrust@uw.edu

Keywords: *Prochlorococcus*, *Synechococcus*, Picoeukaryote, picoplankton, carbon cycle, climate change, biogeochemical provinces, nitrate limitation, Michaelis-Menten

Abstract:

The cyanobacteria *Prochlorococcus* and *Synechococcus* dominate primary production in the tropical marine oceans. Cyanobacterial abundance is expected to increase in future warmer oceans where increased temperature-driven stratification will likely limit inorganic nutrient supply from the deep ocean to surface waters. Large uncertainties in possible outcomes remain, mainly due to limited observational data from these regions. Here we use continuous flow cytometry to obtain incubation-independent estimates of cyanobacteria division rates and abundances of natural populations spanning ~8000km across three different regions in the tropical Atlantic. *Prochlorococcus* division rates appear to be limited by nitrate availability in the South Atlantic Gyre and ammonium in the Western Tropical Atlantic Ocean. From our observations, we derive Michaelis-Menten kinetic models of division rate for *Prochlorococcus* as a function of nitrate and ammonium concentrations in the subtropical and tropical Atlantic respectively. We estimate from *in situ* division rates, abundance and mixed layer gas measurements that cyanobacteria are responsible for ~58-100% of gross primary production in these regions. We hypothesize that nitrate-utilizing ecotypes of *Prochlorococcus* may expand their geographical range in a warming and more strongly stratified ocean, leading to enhanced competition with larger nitrate-utilizing phytoplankton and shifts in community structure.

Introduction:

Increasing atmospheric temperatures are driving increases in ocean surface temperatures (1, 2), a broad-scale change expected to alter ocean ecosystems and biogeochemical cycles (3). Such enhanced surface warming at low latitudes is predicted to increase the geographic range and abundance of the smallest, most abundant marine phytoplankton, the cyanobacteria *Prochlorococcus* and *Synechococcus* (4). Simultaneously, increasing temperature drives ocean stratification and decreases delivery of inorganic nutrients from the deeper ocean to surface ocean communities, which is predicted to exacerbate nutrient-limitation of phytoplankton productivity (5). Resulting shifts in phytoplankton composition favoring species with smaller average cell sizes are expected to decrease the export of phytoplankton carbon from the surface layer to the deeper ocean (6, 7), due, in part, to the slower sinking rates of small particles. Complicating this expectation is recent model-based evidence that small phytoplankton cells can be exported at a rate proportional to their net primary productivity if they form larger particles through aggregation (8). Thus large uncertainties persist in how climate change will alter ecosystem function and carbon export in the globally important tropics and subtropics.

Numerical models provide insights into how phytoplankton community structure is shaped by environmental conditions but these models currently rely on observations of species abundance in the field (4) or physiology data from cultured representatives to constrain division rates and competitive fitness (9, 10). In the tropics, cyanobacteria growth and mortality are nearly perfectly balanced (11, 12) with cell abundance often decoupled from division rate, making abundance patterns complicated to interpret as an indicator of cyanobacteria fitness. Additionally, cyanobacteria across ocean regions may differ substantially in physiology and metabolic capabilities from cultured representatives in the lab due to gene loss and gain (13, 14). Observations of *in situ* growth rates of cyanobacteria across low latitude regions and how they are influenced by environmental factors would help constrain models of community structure and improve our predictive power.

Standard methods for measuring cyanobacteria division rates include dilution experiments (15) and cell cycle analysis (16), both of which are labor intensive approaches, limiting temporal and spatial resolution. Dilution experiments are also potentially biased by the necessity of bottle incubations (17) making these rate measurements subject to large uncertainties. Rather than observing the doubling of DNA as in cell cycle analysis, we use continuous flow cytometry to infer *in situ* division rates based on the change in the size distribution over the diel cycle (18, 19). This size-based method provides accurate estimates of *in situ* division rates of *Synechococcus* (18, 20) and *Prochlorococcus* (19), making it possible to measure cyanobacteria division rates without the bias of bottle incubations and with fine-scale temporal and spatial resolution.

To investigate how temperature and nutrient availability shapes cyanobacteria community structure and biogeochemical cycles in the tropics and subtropics, we pair continuous flow cytometry with other incubation-independent gas measurement-based techniques to estimate phytoplankton gross oxygen production (GOP) and net oxygen production (NOP) in the mixed layer (21, 22). Using the underway flow cytometer, SeaFlow (23), we made continuous observations of phytoplankton populations (~0.2 -

10μm diameter) to estimate division and production rates across a ~8000km transect in the Tropical Atlantic Ocean and compared these with estimates of production and export from mixed layer gas measurements.

Materials/Methods:

Underway measurements were made and discrete samples were collected aboard the R/V Knorr between March and May 2013. Underway data collection was continuous except during passage through Exclusive Economic Zones and when the ship's underway system was bleached to remove biofouling.

Biogeochemical Province Boundaries: Province boundaries were defined by hierarchical clustering of daily average sea surface temperature, chlorophyll *a* fluorescence and salinity similar to the methods of Reygondeau et al. (24). After scaling the data to eliminate differences in units (scale function, stats package R), Euclidean distances were calculated (dist function, stats package R), clustered using Ward's method (hclust function, ward.D, stats package R), and cut at an arbitrary height to yield three clusters (cutree function, k=3, stats package R). Clusters were designated as biogeochemical provinces and named according to their regions as in Longhurst (11).

Flow Cytometry Measurements: Continuous underway flow cytometery measurements were made using SeaFlow (23) by sampling at 5m from the flow-through seawater system of the *R/V* Knorr after filtering through a 100 μm pre-filter. SeaFlow data files were recorded every three minutes. Discrete samples (1.8 mL) were collected from each station from 5m using the Niskin bottles attached to a rosette, and were fixed in a final concentration of 0.5% gluteraldehyde for 20 minutes, flash frozen and stored at −80°C for later analysis. Fixed samples were run on an Influx flow cytometer (Cytopeia/BD Biosciences) and used to independently determine *Prochlorococcus*, *Synechococcus* and picoeukaryote cell abundances.

SeaFlow data processing: SeaFlow data files were processed using the R package *popcycle* version 0.1 (github.com/uwescience/popcycle). Filtering parameters were chosen to retain optimally positioned particles for downstream analysis (defined using a width of 0.2 and a notch of 0.8)(23). Populations of *Prochlorococcus*, *Synechococcus* and picoeukaryotes along with a 1μm bead internal standard were gated manually based on characteristic chlorophyll *a* and phycoerythrin fluorescence, and forward scatter. Aggregate statistics for each population were calculated for each 3-minute file and quality controls were performed to eliminate files with changes in stream pressure exceeding 0.1psi or for outliers likely caused by file writing errors, identified by a ≥15% deviation in cell abundance from a smoothed mean (fourth-order butterworth low pass filter, critical frequency 1 hr^{-1}, R package signal).

Division rate and cell production rate calculations: Division rates of *Prochlorococcus* and *Synechococcus* were estimated using the R scripts *ssPopModel* (github.com/armbrustlab/ssPopModel). Originally developed by Sosik et al. (18) and modified by Ribalet et al. (19), the model fits to the observed cell size distribution over

the course of the day by fitting the cell size/cell division relationships and the light-dependence of cell division to minimize the difference between observed and modeled shifts in cell size distribution for hourly time steps over a 24 hour window. Hourly estimates of cell division were calculated as averages from 24 independent model runs with a one-day rolling window. The precision for model projections was estimated as the standard deviation of 24 hourly model estimates (SD= 0.001-0.023 hr^{-1} or 0.024-0.55 d^{-1}, n=24) and the accuracy was estimated as the standard deviation of the difference between the hourly-observed (based on abundance) and modeled division rate (based on cell size-distribution) of *Prochlorococcus* from a lab culture validation (SD= 0.0029 hr^{-1} or 0.07 d^{-1}, n=42 hours) (19). Daily-integrated division rate was calculated by summing the hourly division rate over 24 hours with uncertainty propagated from the standard deviation of the precision or accuracy (which ever is greater) in hourly division rate estimates. Net carbon production (NPP) was determined by multiplying mean daily-averaged cell abundance by the daily-integrated division rate and estimated carbon biomass per cell estimated from cultured representatives of *Prochlorococcus* (MED4) and *Synechococcus* (WH8012 and WH8103) (53 ± 9 and 170 ± 65 fg C respectively)(25). Uncertainty in NPP was propagated from the standard deviations of mean daily abundance, carbon per cell and daily-integrated division rate (ranging 17-21% for *Prochlorococcus* and 38-64% for *Synechococcus*).

Maximum division rate estimates: Maximum daily-division rates were estimated for the in situ temperature using temperature-dependent growth curves from nutrient-replete cultures of the high light ecotype of *Prochlorococcus* (eMIT9312), found previously to be dominant in the tropical Atlantic (26), and warm water *Synechococcus* (strain WH8103)(27). These temperature-dependent division rates were further corrected for in situ light levels using mean daily photosynthetically active radiation (PAR) in the mixed layer assuming an irradiance attenuation coefficient of 0.05 m^{-1} (28) and irradiance-dependent growth curves from the same strains (27, 29). Uncertainty in maximum growth rates for *Prochlorococcus* was propagated from the standard deviation of daily maximum division rates from cultured strains (http://proportal.mit.edu/pubdownload/papers/pubmed_16556835/index.html).

Nutrient and normalized division rate relationships: Nutrients (estimated precision 0.1% of dynamic range, data available from BCO-DMO, http://www.bco-dmo.org/dataset/473296) were averaged in the mixed layer and interpolated to along-transect distance (R function approx, stats) to determine estimates for nutrient concentrations between stations. Division rates were normalized to *in situ* estimated maximum division rates and compared to inorganic nitrogen concentrations in surface water. Relationships between *in situ* nutrient concentration and normalized division rate were fit to a Michaelis-Menten model of rate (R) and concentration (c) (Equation 1) using a non-linear least-squares regression (R function nls, stats), where Vmax is the maximum rate at saturation and Km is the nutrient concentration at half-saturation.

$$R = \frac{Vmax * c}{(Km + c)} \qquad \text{(Equation 1)}$$

Uncertainty in model fit was propagated from the standard deviation in normalized division rates and nutrient precision (95% confidence interval) by the Monte Carlo

method (R function rnorm, stats), mean and standard deviation of 1000 iterations were calculated for Vmax and Km.

Oxygen/Argon (O_2:Ar) and triple oxygen isotope measurements: Discrete water samples were taken on station at 5m from the Niskin bottles attached to a rosette and at two or more depths below and above the pycnocline to correct for vertical eddy diffusion and seasonal entrainment (30). Samples were collected in evacuated glass flasks with gas-tight valves, with care taken to exclude bubbles during sampling. 100 µL of saturated mercuric chloride solution was added to the flasks during bottle preparation to prevent biological activity after collection. Oxygen (O_2) and Argon (Ar) from the equilibrated headspace of each sample was analyzed on a MAT 253 isotope ratio mass spectrometer using methods similar to those of Barkan and Luz (31) and Reuer et al. (32) as described by Stanley and Howard (33). Corrections were applied for instrument response to sample size and matrix effects, instrument drift, and partitioning between water and headspace in the sample. Ratios of the stable oxygen isotopes (^{18}O, ^{17}O, ^{16}O) were used to calculate the photosynthetic fractionation of oxygen isotopes $^{17}\Delta$ (21). The measured ratio of O_2 to Ar relative to air [$\delta(O_2$:Ar)] was related to the expected ratio of the dissolved gases at equilibrium with the atmosphere (34, 35) to define $\Delta(O_2/Ar)$, the biological oxygen supersaturation (32).

Gas flux and bulk production calculations: Steady-state mass balances for gas exchange processes (36) and transport across the bottom of mixed layer for O_2 and Ar were combined to estimate in situ net oxygen production (NOP, Equation 2) over the residence time of oxygen in the mixed layer (approximately 10-20 days). Mass balances for the triple oxygen isotopic ratios were similarly combined to determine gross oxygen production (GOP, Equation 3) after Prokopenko et al. (37).

$$NOP = k_{O2}*[O_2]_{sat}*\Delta(O_2/Ar)*Ar/Ar_{sat} - C_{entr} - C_{mix} \quad \text{(Equation 2)}$$

$$GOP = [-k_{O2}*[O_2]_{sat}*(^{17}\Delta_{air} - {}^{17}\Delta) - C_{entr} - C_{mix}]/(^{17}\Delta_{photo} - {}^{17}\Delta) \quad \text{(Equation 3)}$$

Where k_{O2} is the gas transfer velocity as a function of wind speed (36), $[O_2]_{sat}$ and Ar_{sat} are the saturated oxygen and argon concentrations at *in situ* temperature and salinity (34), and $^{17}\Delta_{air}$ and $^{17}\Delta_{photo}$ are the atmospheric equilibrium and photosynthetic end-members of the $^{17}\Delta$ tracer (33, 38). Corrections for vertical eddy diffusion (C_{mix}) and seasonal entrainment (C_{entr}) was parameterized after the methods of Nicholson et al. (30) (Equations 4 and 5).

$$C_{mix} = k_z /(Z_{deep}-Z_{ML}) *([O_2]_{deep}*X_{deep} - [O_2]_{ML}*X_{ML}) \quad \text{(Equation 4)}$$

$$C_{ent} = dZ_{ML}/dt *([O_2]_{deep}*X_{deep} - [O_2]_{ML}*X_{ML}) \quad \text{(Equation 5)}$$

Mixed layer depth (Z_{ML}) was defined as a 0.125 kg m^{-3} offset in potential density from the surface (39) and vertical diffusivity (k_z) is assumed to be $3x10^{-5}$ m^2 s^{-1} across the transect (40). Gas samples from profiles collected at the same station from 20m-40m below the mixed layer (Z_{deep}) were used to estimate the mixing gradient of Δ (O_2/Ar) or $^{17}\Delta$ gas tracers (designated as X in Equations 4 and 5) respectively for corrections used in Equations 2 and 3. The time rate of change of the mixed layer depth (dZ_{ML}/dt) was

estimated from the monthly average March-May MIMOC Argo/Model climatology (http://www.pmel.noaa.gov/mimoc/)- no entrainment term was applied when the mixed layer depth decreased or if the change was indistinguishable from zero within errors ($dZ_{ML}/dt \leq 0$). Production rates in units of μmol O_2 L^{-1} d^{-1} were calculated by integrating the gross oxygen production (GOP) over the mixed layer depth and estimates of carbon fixation were made assuming a ratio of GOP (O_2) to net primary production (NPP) of 2.7 compiled from globally distributed 24 hour ^{18}O-GOP/^{14}C-NPP incubations from the Joint Global Ocean Flux Study (JGOFS) (21, 41).

Results/Discussion:

The cruise transect spanned ~8000km of open ocean in the tropical Atlantic Ocean (Figure 1a), crossing through the South Atlantic sub-tropical gyre and the Western tropical Atlantic (11). Due to the dynamic nature (24) of the biogeochemical provinces originally identified by Longhurst (1995), we identified province boundaries at the time of our study based on hierarchical clustering of underway salinity, temperature and chlorophyll *a* fluorescence (Figure 1b). We determined the extent of three provinces: South Subtropical Transition (coolest temperature, intermediate salinity and intermediate chlorophyll *a* fluorescence), South Atlantic Gyre (intermediate temperature, high salinity and low chlorophyll *a* fluorescence), and the Western Tropical Atlantic (highest temperature, low salinity, and high chlorophyll *a* fluorescence). These provinces harbor distinct picophytoplankton communities (Figure 2). *Prochlorococcus* numerically dominates all provinces, but especially so in the South Atlantic Gyre. *Synechococcus* and picoeukaryote populations are much more abundant in the South Subtropical Transition and Western Tropical Atlantic (Figure 2).

We estimated hourly division rates for *Synechococcus* and *Prochlorococcus* based on changes in their cell size distributions over a diel cycle (19, 20) (Supplemental Figure 1) and summed hourly division over 24 hours to calculate daily division rates. As expected, the division rates of cyanobacteria were not correlated with their abundance across the transect (Figure 2, Figure 3a, b), for example *Synechococcus* retained relatively high division rates in the South Atlantic Gyre despite very low abundance. These division rates were then compared to maximum division rates observed with cultured representatives at *in situ* temperature and light levels –the tropical strain *Synechococcus* WH8103 and *Prochlorococcus* eMIT9312, previously shown to dominate this region (42) (Figure 3a, b). We find that our estimated *in situ* division rates for *Synechococcus* were typically lower than WH8103 maximum division rates (Figure 3b). These patterns suggest either wide-spread limitation or that the WH8103 strain is not representative of the *in situ* physiology, as field populations are often composed of multiple phylogenetic groups (43). Although *in situ* division rates of *Synechococcus* appear to be low where nitrate concentrations are low (Figure 3b,c), our interpretation of these patterns is limited by the lack of confidence in applying maximum division rates derived from strain WH8103. In contrast, across most of the transect, *in situ Prochlorococcus* division rates closely match eMIT9312 maximum division rates at the *in situ* temperature and photosynthetically active radiation (PAR) (Figure 3a). Low inorganic nitrogen concentrations were observed where *Prochlorococcus* division rates are lower than predicted by the *in situ* temperature and PAR (Figure 3a, c, d) suggesting that nitrogen

availability limits the growth of *Prochlorococcus* in these regions. These results are consistent with global nutrient-limitation models which predict that picoplankton should be limited by nitrogen in these regions (44).

Low ammonium concentrations in surface waters co-occurred with sub-maximal division rates of *Prochlorococcus* in the Western Tropical Atlantic only, whereas, low nitrate and nitrite co-occurred with sub-maximal *Prochlorococcus* division rates in the S. Subtropical Transition and South Atlantic Gyre (Figure 3a, c, d). The observed differences suggest that *Prochlorococcus* ecotypes with different nitrogen physiologies may inhabit different provinces. Recent work has discovered select *Prochlorococcus* strains with the ability to assimilate nitrate rather than only ammonium as previously thought (13, 45). Furthermore these nitrate-assimilating ecotypes have been found only in very low nitrogen environments similar to the South Atlantic Gyre province (13). Concentrations of *in situ* inorganic nitrogen versus normalized growth rates for *Prochlorococcus* reveal relationships that appear to follow a Michaelis-Menten model (Figure 4), which is expected for these oligotrophic regions where inorganic nutrients are very low in surface waters and phytoplankton growth rates can be limited by kinetics of nutrient uptake (46). The maximum normalized division rate (Vmax parameter) fit to our field data (Table 1) closely matches the predicted maximum growth rate from eMIT9312 particularly in the Western Tropical Atlantic. Additionally, Vmax for *Prochlorococcus* is ~20% lower in the South Atlantic Gyre compared to the Western tropical Atlantic, similar to the 17% decline in division rate observed with *Prochlorococcus* strains grown on nitrate rather than ammonium (45). Our parameter fits also provide an incubation-free estimate of the half-saturation constants (Km) for nitrate and ammonium for *Prochlorococcus*. Our estimated half-saturation constant for nitrate (Km = 6.9 ± 6.9) in the South Atlantic Gyre is lower, but a similar in magnitude to those measured in incubation experiments with natural communities in the subtropical North Atlantic (Km ~20 nM NO_3^-)(47) and about two orders of magnitude lower than measured for larger phytoplankton (46), as would be predicted from the cyanobacteria's relatively large surface area to volume. Previous numerical models (9, 10) assumed both a higher Km (~20 nM compared to our estimated 3.1 ± 2.5 nM) for ammonium than our estimates and importantly that *Prochlorococcus* analogs could only access ammonium. Our *in situ* division rate data corrected for the effects of temperature and light, suggests that *Prochlorococcus* is limited by nitrate in the South Atlantic Gyre and ammonium in the Western Tropical Atlantic. Numerical models could be improved by incorporating these *in situ* derived parameters to more accurately represent the physiology of phytoplankton in the ocean.

The presence of nitrate-assimilating *Prochlorococcus* ecotypes would have important implications for predicting the response of *Prochlorococcus* to enhanced nutrient limitation in this region and the resulting impacts on biogeochemical cycles and ecosystems. The contribution of *Prochlorococcus* and *Synechococcus* to total production in these regions was calculated by multiplying division rates by abundance and estimating carbon per cell. We converted the net primary production (NPP) of the cyanobacteria to gross oxygen production (GOP) assuming a ratio of 2.7 GOP:NPP (41) and compared this to our *in situ* gas-based estimates of total GOP. We find that cyanobacteria could account for ~58-100% of GOP in the mixed layer with

Prochlorococcus dominating production in the South Atlantic Gyre and Western Tropical Atlantic (Table 2). Our estimates suggest that ~87-95% of GOP can be attributed to *Prochlorococcus* in the Western tropical Atlantic and South Atlantic Gyre. Our estimates agree with cell cycle based measurements of *Prochlorococcus*, which found *Prochlorococcus* accounted for ~82% of production in the subtropical North Pacific (16). The ratio of net to gross oxygen production (NOP:GOP), a proxy for the export ratio (48), varied widely within and between biogeochemical provinces in this study (Table 2) and was not correlated with the fraction of cyanobacteria production to total production as we might expect if cyanobacteria were exported at a significantly slower rate than other phytoplankton groups. The ratios we measured in this region of ~0.11-0.34 (NOP:GOP, Table 2) agree with previous estimates from the tropics (21), but the role of cyanobacteria in carbon export remains unclear in these regions despite their dominance of gross production. The Michaelis-Menten relationship between division rates and nitrate in combination with a lower Vmax in the South Atlantic Gyre compared to the Western Tropical Atlantic suggest that *Prochlorococcus* may be primarily utilizing nitrate in the South Atlantic Gyre. However, based on the export ratio (NOP:GOP) in the South Atlantic Gyre, *Prochlorococcus* production in this region cannot be primarily "new" or "export" production from the supply of deep nitrate as classically described by steady-state models (6). Rather, nitrate-utilization by *Prochlorococcus* could be largely recycled production supported by nitrate produced by ammonia oxidizers (estimated to be >70% of nitrate supply in oligotrophic regions) (49).

As surface waters warm, nitrogen availability is expected to become more limiting in the tropics (5) expanding the extent of subtropical gyres and potentially increasing the range of the nitrate-utilizing *Prochlorococcus* ecotype, which is found exclusively in very oligotrophic habitats (13, 45). A wider geographic range for nitrate-utilizing *Prochlorococcus* would increase competition for nitrate among phytoplankton species, favoring *Prochlorococcus* due to its very low half-saturation for nitrate. These results also provide us with predictive power about how division rates will change as these regions warm and become more stratified. Based on cultured representative strains, *Synechococcus* division rates would be ~3-18 % faster in the Southern provinces and ~20% slower in the Western Tropical Atlantic with increased temperature predicted for these regions by 2090 in the RCP8.5 emissions scenario (50). *Prochlorococcus* would be predicted to grow ~30% faster in the South-subtropical transition region and ~10-20% more slowly in the South Atlantic Gyre and Western Tropical Atlantic in the year 2090. Since we find evidence for nitrate-utilizing ecotypes, the decrease in *Prochlorococcus* productivity due to temperature in the South Atlantic Gyre could be exacerbated by increased nitrate-limitation due to stronger stratification predicted for the end of the century.

Conclusions:

Advances in flow cytometry allow collection of continuous, accurate estimates of *in situ* division rates of cyanobacteria. These observations allow us to measure rates of net primary production and estimate the physiology of nutrient limitation of field populations *in situ*. Our observations reveal different relationships of normalized division rate with

nitrate and ammonium for *Prochlorococcus* between biogeochemical provinces. Our findings suggest that *Prochlorococcus* can utilize nitrate in the South Atlantic Gyre, but only ammonium in the Western Tropical Atlantic. These results imply that increasing temperature and stratification may act together to decrease the division rates of the *Prochlorococcus* in the South Atlantic Gyre and potentially shift microbial communities and nitrogen cycling in the tropics.

Acknowledgements: This work was made possible by the Captain and crew of the R/V Knorr, co-principle investigators E. Kujawinski and K. Longnecker, and financial support from the National Science Foundation (OCE-1154320 awarded to E. Kujawinski and K. Longnecker) and Moore Foundation (Grant# awarded to E.V. Armbrust). We gratefully acknowledge M. Schatz for assistance with running fixed flow cytometry samples, J. Swalwell for assistance with SeaFlow set-up and operation, R. Morris and P. Quay for comments on the manuscript and G. Rocap for discussions on data analysis and interpretation.

References:

1. Meehl GA, et al. (2007) *Global climate projections* Available at: http://www.ipcc.ch/publications_and_data/ar4/wg1/en/ch10.html [Accessed November 9, 2011].

2. Ciais P, et al. (2013) *Carbon and Other Biogeochemical Cycles. In: Climate Change 2013: The Physical Science Basis* (Cambridge, United Kingdom).

3. Riebesell U, Körtzinger A, Oschlies A (2009) Sensitivities of marine carbon fluxes to ocean change. *Proc Natl Acad Sci U S A* 106(49):20602–9. Available at: http://www.pubmedcentral.nih.gov/articlerender.fcgi?artid=2791567&tool=pmcentrez&rendertype=abstract.

4. Flombaum P, et al. (2013) Present and future global distributions of the marine Cyanobacteria Prochlorococcus and Synechococcus. *Proc Natl Acad Sci U S A*:1–6. Available at: http://www.ncbi.nlm.nih.gov/pubmed/23703908 [Accessed May 25, 2013].

5. Moore JK, Lindsay K, Doney SC, Long MC, Misumi K (2013) Marine ecosystem dynamics and biogeochemical cycling in the community earth system model [CESM1(BGC)]: Comparison of the 1990s with the 2090s under the RCP4.5 and RCP8.5 scenarios. *J Clim* 26(23):9291–9312.

6. Eppley R, Peterson BJ (1979) Particulate organic matter flux and planktonic new production in the deep ocean. *Nature* 282(677-680). Available at:

http://iod.ucsd.edu/courses/sio280/documents/eppley_peterson_79_f_ratio_nature.pdf [Accessed November 7, 2011].

7. Michaels AF, Silver MW (1988) Primary production , sinking fluxes and the microbial food web. *Deep Res* 35(4):473–490.

8. Richardson TL, Jackson G a (2007) Small phytoplankton and carbon export from the surface ocean. *Science* 315(5813):838–40. Available at: http://www.ncbi.nlm.nih.gov/pubmed/17289995 [Accessed October 29, 2012].

9. Follows MJ, Dutkiewicz S, Grant S, Chisholm SW (2007) Emergent biogeography of microbial communities in a model ocean. *Science* 315(5820):1843–6. Available at: http://www.ncbi.nlm.nih.gov/pubmed/17395828 [Accessed October 6, 2012].

10. Dutkiewicz S, Follows MJ, Bragg JG (2009) Modeling the coupling of ocean ecology and biogeochemistry. *Global Biogeochem Cycles* 23(4):GB4017. Available at: http://www.agu.org/pubs/crossref/2009/2008GB003405.shtml [Accessed February 28, 2013].

11. Longhurst A (1995) Seasonal cycles of pelagic production and consumption. *Prog Oceanogr* 36(2):77–167. Available at: http://linkinghub.elsevier.com/retrieve/pii/0079661195000151.

12. Liu H, Campbell L, Landry MR (1995) Growth and mortality rates of Prochlorococcus and Synechococcus measured with a selective inhibitor technique. *Mar Ecol Prog Ser* 1:277–287.

13. Martiny AC, Kathuria S, Berube PM (2009) Widespread metabolic potential for nitrite and nitrate assimilation among Prochlorococcus ecotypes. *Proc Natl Acad Sci U S A* 106(26):10787–92. Available at: http://www.pubmedcentral.nih.gov/articlerender.fcgi?artid=2705535&tool=pmcentrez&rendertype=abstract.

14. Saunders JK, Rocap G Genomic potential for arsenic efflux and methylation varies among global Prochlorococcus populations. *ISME J*.

15. Landry M, Kirshtein J, Constantinou J (1995) A refined dilution technique for measuring the community grazing impact of microzooplankton, with experimental tests in the central equatorial Pacific. *Mar Ecol Prog Ser* 120:53–63. Available at: http://www.int-res.com/abstracts/meps/v120/p53-63/.

16. Liu H, Nolla HA, Campbell L (1997) Prochlorococcus growth rate and contribution to primary production in the equatorial and subtropical North Pacific Ocean. *Aquat Microb Ecol* 12:39–47.

17. Worden A, Binder B (2003) Application of dilution experiments for measuring growth and mortality rates among Prochlorococcus and Synechococcus populations in oligotrophic environments. *Aquat Microb Ecol* 30:159–174. Available at: http://www.int-res.com/abstracts/ame/v30/n2/p159-174/.

18. Sosik HM, Olson RJ, Neubert MG, Shalapyonok A, Solow AR (2003) Growth rates of coastal phytoplankton from time-series measurements with a submersible flow cytometer. *Limnol Oceanogr* 48(5):1756–1765. Available at: http://www.aslo.org/lo/toc/vol_48/issue_5/1756.html.

19. Ribalet F, et al. (2015) Light-driven synchrony of *Prochlorococcus* growth and mortality in the subtropical Pacific gyre. *Proc Natl Acad Sci* (November 2011):201424279. Available at: http://www.pnas.org/lookup/doi/10.1073/pnas.1424279112.

20. Hunter-Cevera KR, et al. (2014) Diel size distributions reveal seasonal growth dynamics of a coastal phytoplankter. *Proc Natl Acad Sci U S A* 111(27):1–6. Available at: http://www.ncbi.nlm.nih.gov/pubmed/24958866 [Accessed July 9, 2014].

21. Juranek LW, Quay PD (2011) Using Triple Isotopes of Dissolved Oxygen to Evaluate Global Marine Productivity. *Ann Rev Mar Sci* 5:120820103326000.

22. Luz B, Barkan E (2009) Net and gross oxygen production from O2/Ar, 17O/ 16O and 18O/16O ratios. *Aquat Microb Ecol* 56(2-3):133–145.

23. Swalwell JE, Ribalet F, Armbrust EV (2011) SeaFlow: A novel underway flow-cytometer for continuous observations of phytoplankton in the ocean. *Limnol Oceanogr Methods* 9:466–477. Available at: http://www.aslo.org/lomethods/free/2011/0466.html [Accessed January 3, 2013].

24. Reygondeau G, et al. (2013) Dynamic biogeochemical provinces in the global ocean. *Global Biogeochem Cycles* 27(August):1046–1058.

25. Bertilsson S, Berglund O, Karl DM, Chisholm SW (2003) Elemental composition of marine Prochlorococcus and Synechococcus: Implications for the ecological stoichiometry of the sea. *Limnol Oceanogr* 48(5):1721–1731.

26. Johnson ZI, et al. (2006) Niche partitioning among Prochlorococcus ecotypes along ocean-scale environmental gradients. *Science* 311(5768):1737–40. Available at: http://www.ncbi.nlm.nih.gov/pubmed/16556835 [Accessed November 7, 2013].

27. Moore LR, Goericke R, Chisholm SW (1995) Comparative physiology of Synechococcus and Prochlorococcus: influence of light and temperature on growth, pigments, fluorescence and absorptive properties. *Mar Ecol Prog Ser* 116:259–275.

28. Stenz DA (1975) *A Chronological Study of the Measurement of the Optical Properties of Ocean Water and an Atlas of the Diffuse Attenuation Coefficient, "k", of Tropical Atlantic Ocean Water.* (Monerey, CA, USA).

29. Moore LR, Chisholm SW (1999) Photophysiology of the marine cyanobacterium Prochlorococcus: Ecotypic differences among cultured isolates. *Limnol Oceanogr* 44(3):628–638.

30. Nicholson D, Stanley RHR, Doney SC (2014) The triple oxygen isotope tracer of primary productivity in a dynamic ocean model. *Glob Biogeochem Cycles* 28:538–552.

31. Barkan E, Luz B (2005) High precision measurements of 17O/16O and 18O/16O ratios in H2O. *Rapid Commun Mass Spectrom* 19(24):3737–42. Available at: http://www.ncbi.nlm.nih.gov/pubmed/16308852 [Accessed March 20, 2012].

32. Reuer MK, Barnett B a., Bender ML, Falkowski PG, Hendricks MB (2007) New estimates of Southern Ocean biological production rates from O2/Ar ratios and the triple isotope composition of O2. *Deep Sea Res Part I Oceanogr Res Pap* 54(6):951–974. Available at: http://linkinghub.elsevier.com/retrieve/pii/S0967063707000489 [Accessed July 19, 2012].

33. Stanley RHR, Howard EM (2013) Quantifying photosynthetic rates of microphytobenthos using the triple isotope composition of dissolved oxygen. *Limnol Oceanogr Methods* 11:360–373.

34. Garcia H, Gordon LI (1992) Oxygen solubility in seawater : Better fitting equations. *Limnol Oceanogr* 37(6):1307–1312.

35. Hamme RC, Emerson SR (2004) The solubility of neon, nitrogen and argon in distilled water and seawater. *Deep Res Part I Oceanogr Res Pap* 51(11):1517–1528.

36. Stanley RHR, Jenkins WJ, Lott DE, Doney SC (2009) Noble gas constraints on air-sea gas exchange and bubble fluxes. *J Geophys Res Ocean* 114(11):1–14.

37. Prokopenko MG, Pauluis OM, Granger J, Yeung LY (2011) Exact evaluation of gross photosynthetic production from the oxygen triple-isotope composition of O 2 : Implications for the net-to-gross primary production ratios. *Geophys Res Lett* 38(14):n/a–n/a. Available at: http://doi.wiley.com/10.1029/2011GL047652 [Accessed March 8, 2013].

38. Nicholson DP (2011) Comment on: "Technical note: Consistent calculation of aquatic gross production from oxygen triple isotope measurements" by Kaiser

(2011). *Biogeosciences* 8(10):2993–2997. Available at: http://www.biogeosciences.net/8/2993/2011/.

39. Levitus S (1982) Climatological Atlas of the World Ocean. 1–173.

40. Mouriño-Carballido B, et al. (2011) Importance of N2 fixation vs. nitrate eddy diffusion along a latitudinal transect in the Atlantic Ocean. *Limnol Oceanogr* 56(3):999–1007.

41. Marra J (2002) Approaches to the measurement of plankton production. *Phytoplankton Productivity: Carbon Assimilation in Marine and Freshwater Ecosystems* (Blackwell Science, Oxford, UK), pp 78–108.

42. Johnson ZI, et al. (2006) Niche partitioning among Prochlorococcus ecotypes along ocean-scale environmental gradients. *Science* 311(March):1737–1740.

43. Ahlgren N a., Rocap G (2012) Diversity and distribution of marine Synechococcus: Multiple gene phylogenies for consensus classification and development of qPCR assays for sensitive measurement of clades in the ocean. *Front Microbiol* 3(JUN):1–24.

44. Moore JK, Doney SC, Glover DM, Fung IY (2002) Iron cycling and nutrient-limitation patterns in surface waters of the World Ocean. *Deep Sea Res Part II Top Stud Oceanogr* 49:463–507.

45. Berube PM, et al. (2014) Physiology and evolution of nitrogen acquisition in Prochlorococcus. *ISME* 9(5):1195–1207. Available at: http://dx.doi.org/10.1038/ismej.2014.211.

46. Eppley RW, Rogers JN, Mccarthy JJ (1969) Half-saturation constants for uptake of nitrate and ammonium by marine phytoplankton. *Limnol Oceanogr* 14(6):912–920.

47. Harrison WG, Harris LR, Irwin BD (1996) The kinetics of nitrogen utilization in the oceanic mixed layer: Nitrate and ammonium interactions at nanomolar concentrations. *Limnol Oceanogr* 41(1):16–32.

48. Laws E a, et al. (2000) Carbon cycling in primary production bottle incubations: inferences from grazing experiments and photosynthetic studies using and in the Arabian Sea. *Deep Sea Res Part II Top Stud Oceanogr* 47(7-8):1339–1352. Available at: http://linkinghub.elsevier.com/retrieve/pii/S0967064599001460.

49. Yool A, Martin AP, Fernández C, Clark DR (2007) The significance of nitrification for oceanic new production. *Nature* 447(7147):999–1002.

50. Hoegh-Guldberg O, et al. (2014) *The Ocean. In: Climate Change 2014: Impacts, Adaptation, and Vulnerability. Part B: Regional Aspects. Contribution of Working Group II to the Fifth Assessment Report of the Intergovernmental Panel on Climate Change* (Cambridge, United Kingdom).

Table 1: Michaelis-Menten parameter fits for *Prochlorococcus*.
The non-linear least squares fit for Michaelis-Menten parameters (Figure 4) from *in situ* nutrient concentration (nM) v. normalized division rate (dr/dr_{max}) for nitrate (NO_3^-) in the South Subtropical Transition and South Atlantic Gyre and for ammonium (NH_4^+) in the Western Tropical Atlantic. Parameter fits (mean ± SD) estimated by Monte Carlo procedure (1000 iterations).

Nutrient	**Parameter**	**mean ± SD**
NO_3^-	Vmax (dr/dr_{max})	0.87 ± 0.08
	Km (nM)	6.9 ± 6.9
NH_4^+	Vmax (dr/dr_{max})	1.11 ± 0.10
	Km (nM)	3.1 ± 2.5

Table 2: Cyanobacteria dominate mixed layer production across the tropical and subtropical Atlantic.

Net primary production (NPP) of cyanobacteria (mean ± sd) in the mixed layer of the South Subtropical Transition, South Atlantic Gyre and Western tropical Atlantic provinces (n= 6, 12, 18 respectively) is converted to gross oxygen production (GOP). The total mixed layer GOP estimated from triple oxygen isotopes (mean ± sd, n= 5, 6, 5 respectively) in the same provinces, with the fraction of total GOP accounted for by cyanobacteria (mean ± sd) and the ratio of net to gross oxygen production (NOP:GOP) in the mixed layer estimated from triple oxygen isotopes and O_2:Ar (mean ± sd).

Biogeochemical Province		**NPP** μg C L^{-1} d^{-1}	**GOP** μmol O_2 L^{-1} d^{-1}	**Total GOP** μmol O_2 L^{-1} d^{-1}	**Fraction of total GOP**		**NOP:GOP**
South Subtropical Transition	*Prochlorocccus*	2.72 ± 0.66	0.61± 0.15	1.81 ± 0.96	0.34 ± 0.20	0.58 ± 0.31	0.23 ± 0.10
	Synechococcus	1.95 ± 1.63	0.44 ± 0.37		0.24 ± 0.24		
South Atlantic Gyre	*Prochlorocccus*	4.57 ± 1.37	1.03 ± 0.31	1.08 ± 0.61	0.95 ± 0.60	0.97 ± 0.60	0.11 ± 0.06
	Synechococcus	0.10 ± 0.06	0.02 ± 0.01		0.02 ± 0.01		
Western Tropical Atlantic	*Prochlorocccus*	5.70 ± 1.24	1.28 ± 0.28	1.47 ± 0.28	0.87 ± 0.25	1.05 ± 0.28	0.34 ± 0.36
	Synechococcus	1.18 ± 0.77	0.27 ± 0.17		0.18 ± 0.12		

Figure Legends:

Figure 1: Biogeochemical provinces from 2013 tropical Atlantic transect. (a) Daily position colored by hierarchical cluster assignment and overlaid on satellite derived monthly composite for April 2013 chlorophyll *a* (Aqua MODIS) colored according to biogeochemical province as in (b). (b) Hierarchical clustering dendrogram of mean daily underway salinity, temperature and chlorophyll *a* fluorescence; clusters are labeled with biogeochemical province name.

Figure 2: Abundance of picophytoplankton populations in biogeochemical provinces of the tropical Atlantic. Underway flow cytometry derived abundance (10^6 cells L^{-1}) over time along the transect of three populations of picoplankton: *Prochlorococcus* (blue), *Synechococcus* (orange) and picoeukaryotes (green) (hourly mean ± SD in lighter shade, n=20). Dashed lines indicate the boundaries between biogeochemical provinces with the province names indicated above the figure.

Figure 3: *Prochlorococcus* and *Synechococcus* division rates and nitrogen availability. Division rates of *Prochlorococcus* (a) and *Synechococcus* (b) over time along the transect (daily division rate ± SD); colors indicate biogeochemical provinces: South Subtropical Transition (magenta), South Atlantic Gyre (blue), Western Tropical Atlantic (yellow); dashed lines indicate estimated maximum division rate from in situ temperature and PAR. Inorganic nitrogen concentrations (c,d) along the transect were interpolated from surface to 250m depth and then to along track distance from cast samples (black points), color bars indicate concentrations of (c) nitrate + nitrite and (d) ammonium (μM).

Figure 4: Michaelis-Menten curve fits for *Prochlorococcus* within biogeochemical provinces. Concentrations of (a) nitrate + nitrite and (b) ammonium (μM, mean ± estimated precision) versus normalized division rates (dr/dr_{max}, mean ± SD) fit to a Michaelis-Menten equation using non-linear least squares regression. Grey line indicates division rate equal to estimated max division rate, dashed lines indicate estimated standard deviation of Michaelis-Menten fit (Table 2), and colors indicate biogeochemical provinces as in Figure 4.

Supplemental Figure 1: Diel Cycles of Mean Cell Volume and Division Rate for *in situ Prochlorococcus* and *Synechococcus*. The mean forward scatter (mean ± SD, n=20) of *Prochlorococcus* (blue) and *Synechococcus* (orange) populations *in situ* (a,b) over representative light/dark cycles (night indicated by grey bars). The hourly division rate for *Prochlorococcus* and *Synechococcus* (c,d) (mean ± SD, n=24) based on the model fit to population shifts in cell volume indicated by forward scatter.

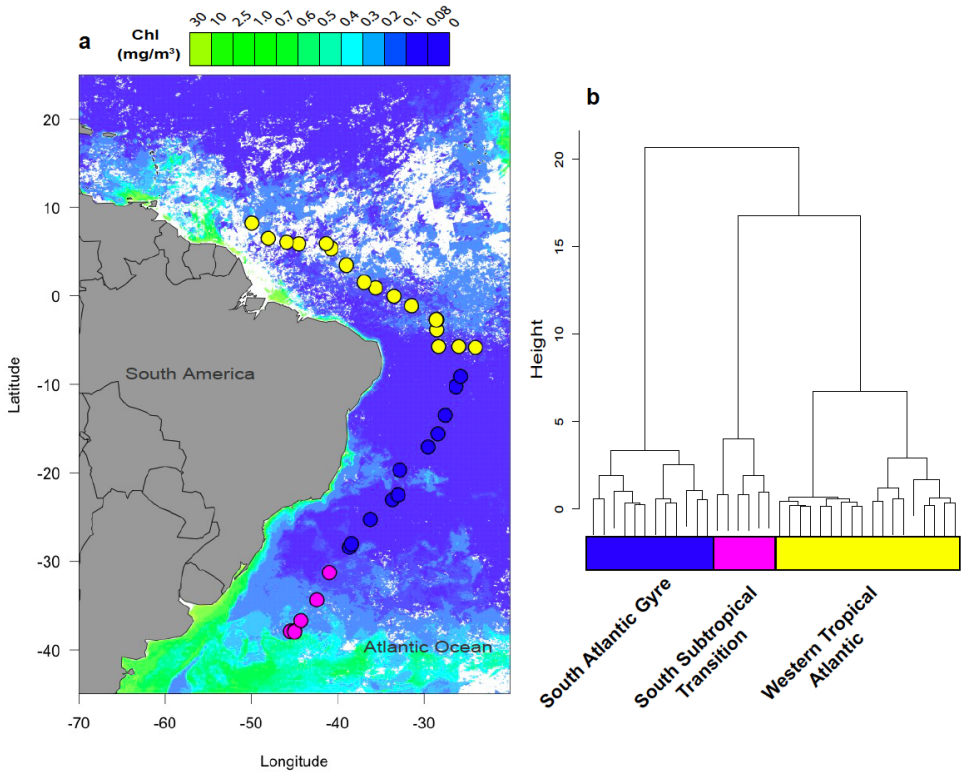
a
Chl
(mg/m³)
30
10
2.5
1.0
0.7
0.6
0.5
0.4
0.3
0.2
0.1
0.08
0
South America
Atlantic Ocean
Latitude
Longitude
20
10
0
-10
-20
-30
-40
-70
-60
-50
-40
-30
b
Height
20
15
10
5
0
South Atlantic Gyre
South Subtropical Transition
Western Tropical Atlantic

Figure 1

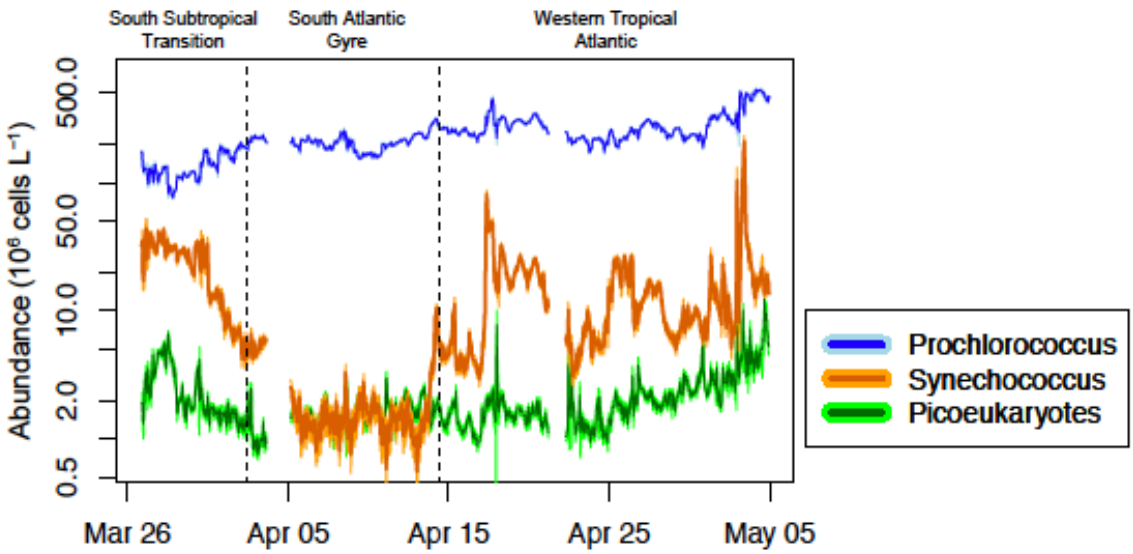
South Subtropical Transition
South Atlantic Gyre
Western Tropical Atlantic
Abundance (10^6 cells L^{-1})
500.0
50.0
10.0
2.0
0.5
Mar 26
Apr 05
Apr 15
Apr 25
May 05
Prochlorococcus
Synechococcus
Picoeukaryotes

Figure 2

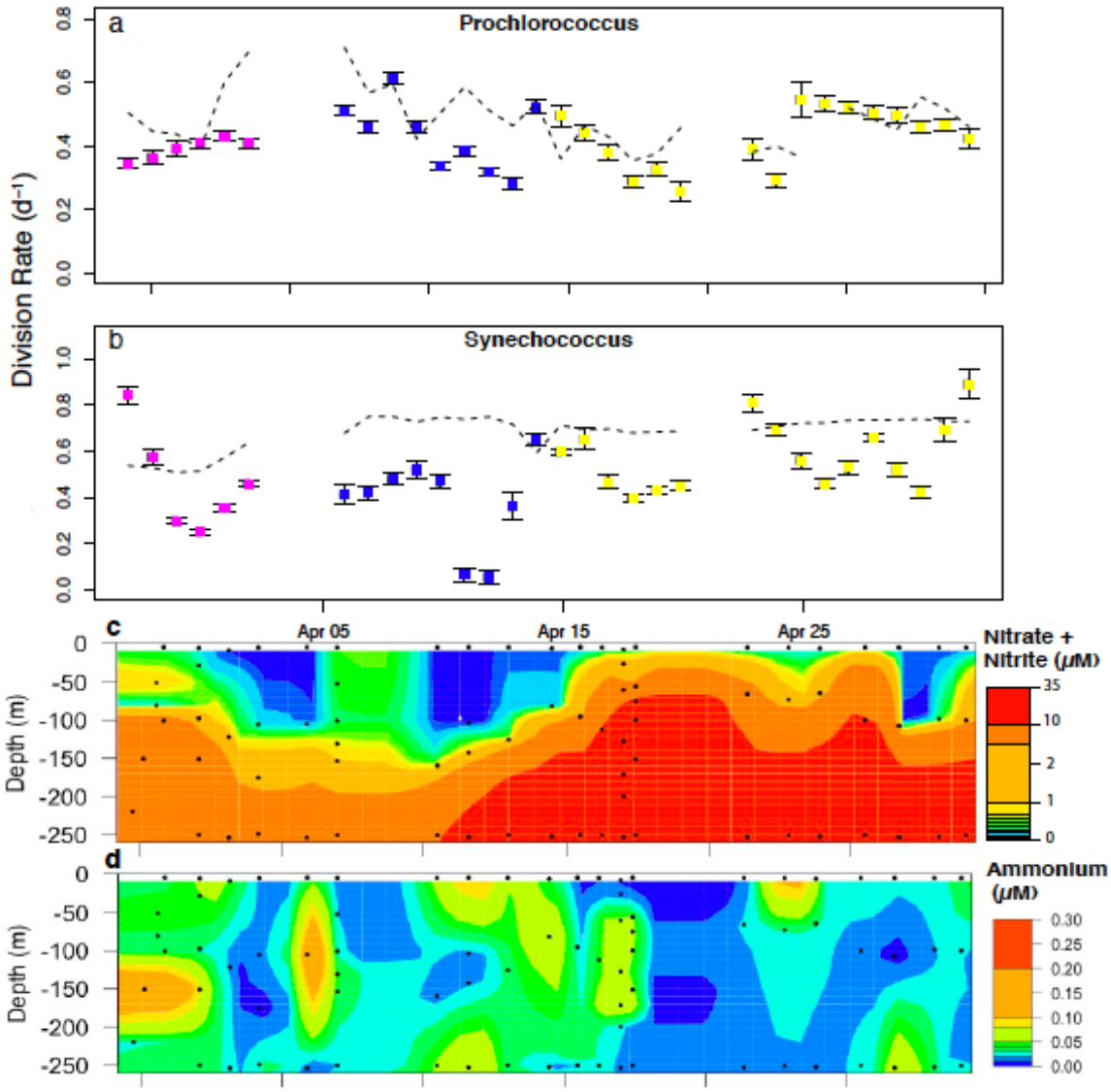
a
Prochlorococcus
Division Rate (d⁻¹)
0.0
0.2
0.4
0.6
0.8
b
Synechococcus
0.0
0.2
0.4
0.6
0.8
1.0
c
Apr 05
Apr 15
Apr 25
Depth (m)
0
-50
-100
-150
-200
-250
Nitrate +
Nitrite (μM)
35
10
2
1
0
d
Depth (m)
0
-50
-100
-150
-200
-250
Ammonium
(μM)
0.30
0.25
0.20
0.15
0.10
0.05
0.00

Figure 3

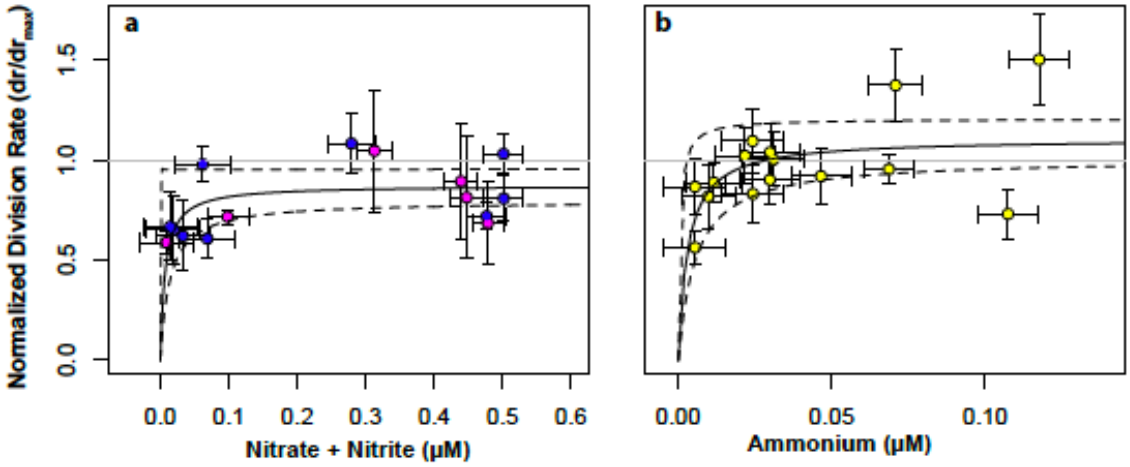
a
b
Normalized Division Rate (dr/dr$_{max}$)
0.0
0.5
1.0
1.5
0.0
0.1
0.2
0.3
0.4
0.5
0.6
Nitrate + Nitrite (µM)
0.00
0.05
0.10
Ammonium (µM)

Figure 4

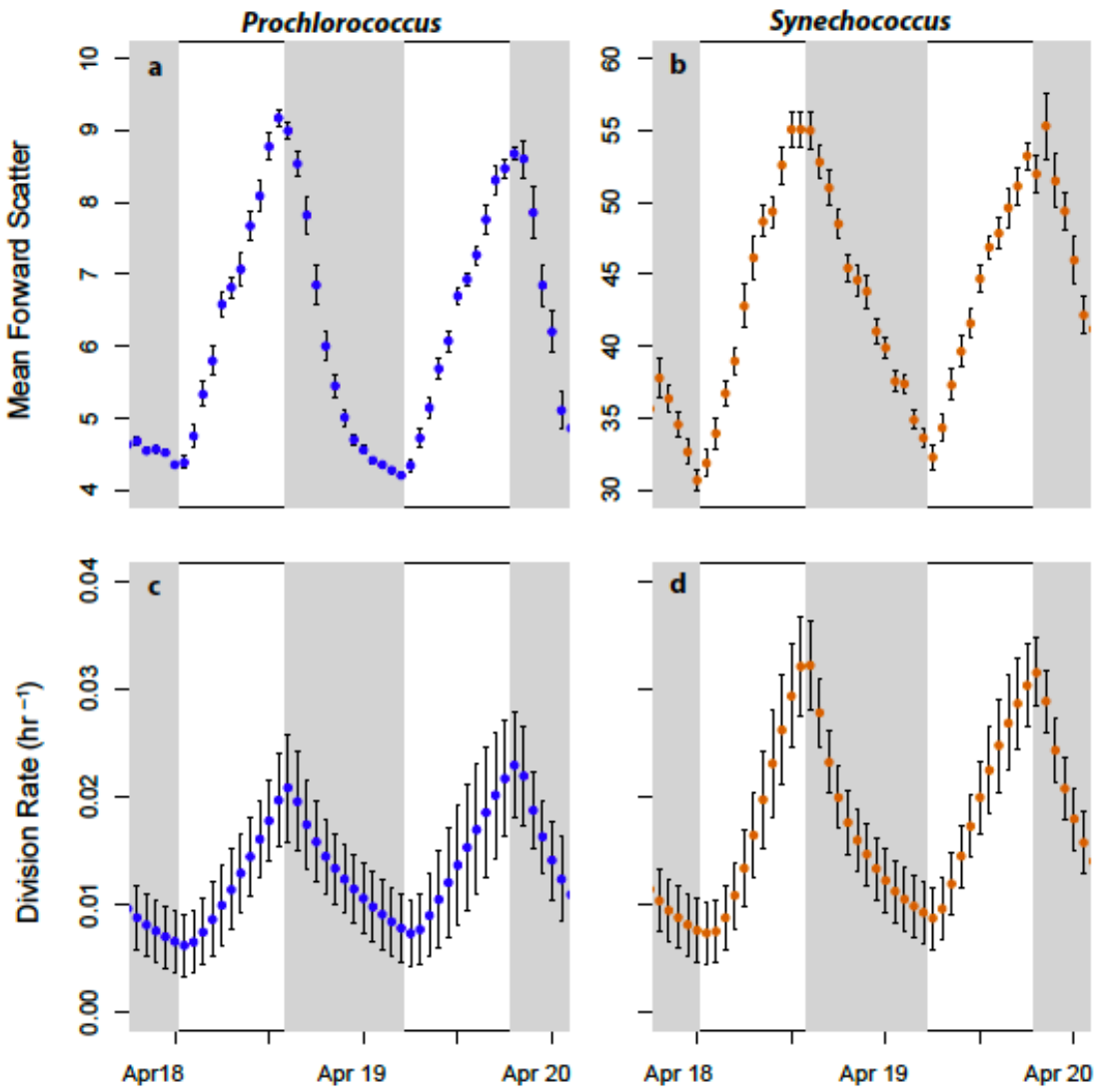

Supplemental Figure 1

Conclusion

Phytoplankton compose the base of the marine food web and fix carbon in the surface ocean, driving the biological pump[1]. Understanding how phytoplankton physiology and community structure will shift in response to the changing climate is essential in predicting changes to global fisheries and the marine carbon cycle[2]. In uncovering mechanisms of phytoplankton response to climate change, we present several important new findings that can inform models of community structure and biogeochemistry.

In investigating the response of a model diatom to elevated CO_2 under nitrate limitation, we found that after acclimation diatoms reorganize cellular metabolism to decrease photosynthesis and respiration as a result of energy savings from down-regulation of the carbon concentrating mechanism (CCM)[3]. The short term response of the diatom to rising CO_2 was much different than the eventual acclimated response, with a shift to high carbon to nitrogen ratios only found in the short term response to CO_2[3]. Different gene groups were also activated by short and long term exposures to elevated CO_2 with a decrease in expression of photosynthesis and respiration genes only seen after longer exposures[4]. These findings suggest that in an ocean with higher CO_2 concentrations, phytoplankton limited by nitrogen availability are likely to decrease the rate of photosynthetic oxygen production while maintaining the same rate of carbon fixation and the same ratio of carbon to nitrogen due to metabolic rearrangement.

We also uncovered a mechanism of how the model diatom *T. pseudonana* senses and acclimates to changing CO_2. CCM and photorespiration genes were linked by a common regulatory pathway controlled by the small molecule signaling intermediate

cyclic-AMP (cAMP) likely produced by a CO_2-responsive cyclase[4]. This CO_2-regulation pathway is likely to be a shared trait across all diatoms that evolved at least 150 million years ago[5], since a similar cAMP-dependent regulatory mechanism was previously discovered in a distantly related diatom *P. tricornutum*[6]. The genes (eg: transcription factors, cyclases, and hypothetical genes) linked to the CO_2-response by this study[4] can serve as targets for future studies on diatom adaptation to rising CO_2 or be used as biomarkers of phytoplankton acclimation to rising CO_2 in the field.

Moving to the field and using continuous flow cytometry[7], we were able to characterize the *in situ* physiology and division rates of the most abundant photosynthetic organisms on the planet, cyanobacteria. Our study site covered ~8000 km of the Atlantic Ocean, ranging from the subtropics to the tropics[8]. We found the division rates of *Prochlorococcus* in these regions to be mostly controlled by sea surface temperature and well represented by the cultured representative strain MIT9312. The controls on the division rates of *Synechococcus* populations were not well represented by lab cultures or were too diverse to be represented by a single model strain. Studies such as this can determine if we are missing good cultured representatives for natural populations and inform phytoplankton community models about the appropriate assumptions.

Although we found temperature to be an important control on the growth of *Prochlorococcus*, nitrogen limitation also affected division rates and varied between the tropics and subtropics. We found apparent nitrate-limitation for *Prochlorococcus* in the subtropical gyre and ammonium-limitation for *Prochlorococcus* in the tropics[8]. These findings suggest different ecotypes are present in these ocean regions and that nitrate-utilizing ecotypes will likely increase in importance in the decades to come as the ocean

becomes more strongly stratified and vertical nutrient fluxes slow. The presence of different ecotypes across regions points to the importance of using competitive fitness models[9] to explore the trade-offs of different ecotypes and where they are likely to be successful in the future oceans.

Given the complexity of predicting how marine communities will respond to changing climate over the coming decades, the problem requires a multi-faceted approach. By studying model organisms in the lab one can uncover mechanisms of physiological and gene expression changes in response to environmental change. These insights can be generalized, but must also be confirmed, if possible, on field populations. Studying field populations is essential as it may uncover important metabolic and physiological diversity, which was previously under represented by lab cultures and can affect the projected response of phytoplankton to climate change.

1. Ducklow, H. W., Steinberg, D. K. & Buesseler, K. O. Upper Ocean Carbon Export and the Biological Pump. *Oceanography* **14,** 50–58 (2001).

2. Riebesell, U., Körtzinger, A. & Oschlies, A. Sensitivities of marine carbon fluxes to ocean change. *Proc. Natl. Acad. Sci. U. S. A.* **106,** 20602–9 (2009).

3. Hennon, G. M. M., Quay, P., Morales, R. L., Swanson, L. M. & Armbrust, E. V. Acclimation conditions modify physiological response of the diatom *Thalassiosira pseudonana* to elevated CO_2 concentrations in a nitrate-limited chemostat. *J. Phycol.* **253,** 243–253 (2014).

4. Hennon, G. M. M. *et al.* Diatom acclimation to elevated CO2 via cAMP signalling and coordinated gene expression. *Nat. Clim. Chang.* **5,** (2015).

5. Armbrust, E. The life of diatoms in the world's oceans. *Nature* **459,** 185–192 (2009).

6. Harada, H., Nakajima, K., Sakaue, K. & Matsuda, Y. CO2 sensing at ocean surface mediated by cAMP in a marine diatom. *Plant Physiol.* **142,** 1318–28 (2006).

7. Swalwell, J. E., Ribalet, F. & Armbrust, E. V. SeaFlow: A novel underway flow-cytometer for continuous observations of phytoplankton in the ocean. *Limnol. Oceanogr. Methods* **9,** 466–477 (2011).

8. Hennon, G. M. M., Howard, E., Stanley, R., Ribalet, F. & Armbrust, E. V. In situ division rates of Prochlorococcus reveal different nitrogen-utilizing ecotypes across the tropical Atlantic. *prep PNAS*

9. Follows, M. J., Dutkiewicz, S., Grant, S. & Chisholm, S. W. Emergent biogeography of microbial communities in a model ocean. *Science* **315,** 1843–1846 (2007).